Cell Reports

Article

Escape steering by cholecystokinin peptidergic signaling

Graphical abstract

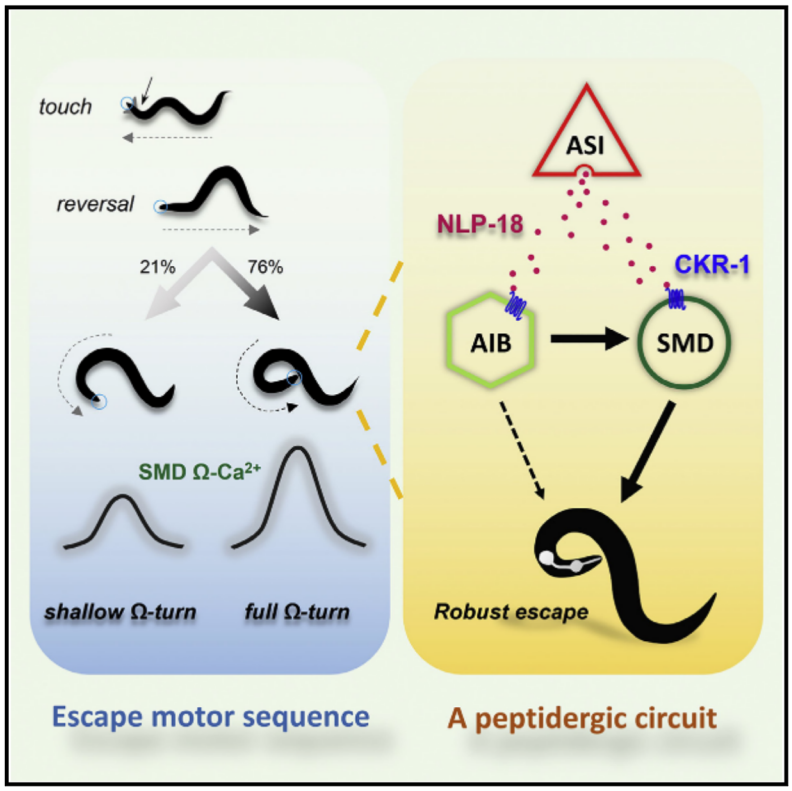

Authors

Lili Chen, Yuting Liu, Pan Su, ...,
Heng Mao, Mei Zhen, Shangbang Gao

Correspondence

sgao@hust.edu.cn

In brief

Escape is a fast innate behavior that is most generated by hard-wired circuits. Chen et al. identify the peptide NLP-18 and its receptor CKR-1, a Gαq-protein-coupled receptor, to form an essential signaling pathway for full Ω turn. Thus, cholecystokinin peptidergic signaling modulates an escape circuit to generate robust escape steering

Highlights

- A neuropeptide NLP-18 secreted by ASI sensory neuron enables full Ω turn during escape
- A $G\alpha_q$-protein-coupled cholecystokinin receptor CKR-1 promotes robust escape steering
- SMD neurons exhibit NLP-18-CKR-1-dependent activity increase during the full Ω turn
- CKR-1 is a cognate receptor of NLP-18

Chen et al., 2022, Cell Reports *38*, 110330
February 8, 2022
https://doi.org/10.1016/j.celrep.2022.110330

CellPress

Cell Reports

CellPress
OPEN ACCESS

Article

Escape steering by cholecystokinin peptidergic signaling

Lili Chen,[1,6] Yuting Liu,[1,6] Pan Su,[1] Wesley Hung,[2] Haiwen Li,[3,4] Ya Wang,[1] Zhongpu Yue,[1] Ming-Hai Ge,[1] Zheng-Xing Wu,[1] Yan Zhang,[1] Peng Fei,[5] Li-Ming Chen,[1] Louis Tao,[3] Heng Mao,[4] Mei Zhen,[2] and Shangbang Gao[1,7,*]

[1]Key Laboratory of Molecular Biophysics of the Ministry of Education, College of Life Science and Technology, Huazhong University of Science and Technology, Wuhan 430074, P.R. China
[2]Lunenfeld-Tanenbaum Research Institute, Mount Sinai Hospital, University of Toronto, Toronto, ON M5G 1X5, Canada
[3]Center for Quantitative Biology, Peking University, Beijing 100871, P.R. China
[4]LMAM, School of Mathematical Sciences, Peking University, Beijing 100871, P.R. China
[5]School of Optical and Electronic Information, Wuhan National Laboratory for Optoelectronics, Huazhong University of Science and Technology, Wuhan 430074, P.R. China
[6]These authors contributed equally
[7]Lead contact
*Correspondence: sgao@hust.edu.cn
https://doi.org/10.1016/j.celrep.2022.110330

SUMMARY

Escape is an evolutionarily conserved and essential avoidance response. Considered to be innate, most studies on escape responses focused on hard-wired circuits. We report here that a neuropeptide NLP-18 and its cholecystokinin receptor CKR-1 enable the escape circuit to execute a full omega (Ω) turn. We demonstrate *in vivo* NLP-18 is mainly secreted by the gustatory sensory neuron (ASI) to activate CKR-1 in the head motor neuron (SMD) and the turn-initiating interneuron (AIB). Removal of NLP-18 or CKR-1 or specific knockdown of CKR-1 in SMD or AIB neurons leads to shallower turns, hence less robust escape steering. Consistently, elevation of head motor neuron (SMD)'s Ca^{2+} transients during escape steering is attenuated upon the removal of NLP-18 or CKR-1. *In vitro*, synthetic NLP-18 directly evokes CKR-1-dependent currents in oocytes and CKR-1-dependent Ca^{2+} transients in SMD. Thus, cholecystokinin peptidergic signaling modulates an escape circuit to generate robust escape steering.

INTRODUCTION

Small invertebrate circuits have provided fundamental insights on conserved circuit principles and neuromodulation that underlie locomotory behaviors (Friedrich, 2013; Friesen and Kristan, 2007; Katz, 2016). Escape, a nociceptive response to steer away from a threat that an animal encounters during foraging, has been a particularly attractive model of ethologically important sensorimotor transformations. Escape occurs fast and exhibits robust stereotypy across species (Chalfie and Jorgensen, 1998; Harris-Warrick, 2011; Wang et al., 2020). For example, looming stimuli, which represent objects on a collision course, initiate robust escape responses across vertebrates and invertebrates (Fotowat and Gabbiani, 2011).

Caenorhabditis elegans (*C. elegans*) employs dedicated circuits for escaping various threats, ranging from predacious fungi (Maguire et al., 2011; Pirri and Alkema, 2012) to nociceptive stimuli (Chalfie et al., 1985; Hilliard et al., 2005). Its escape steering consists of a highly orchestrated sequence of motor actions (Pirri et al., 2009; Wang et al., 2020). A strong mechanical touch to its head, for example, initiates a reversal followed by a head-led, ventral-biased turn that allows the animal to reorient its foraging trajectory. A detailed wiring diagram (White et al., 1986) guided the laser ablation studies that delineate neuronal components of the *C. elegans* navigation motor circuit (Chalfie et al., 1985; Gray et al., 2005; Wicks et al., 1996). Key circuit components for the escape response are mechano- and chemo-sensory neurons that detect noxious stimuli, descending synapses that activate head motor neurons for neck muscles, and ventral-cord-projecting premotor interneurons that regulate motor neurons along the body. Separate motor modules, consisting of interneurons and motor neurons, execute the sequential escape motor steps: reversal (interneurons AVA and AIB); turn (motor neurons SMD and RIV); and forward (interneurons RIB and AVB). Chemical and electrical synaptic connections between neurons of these modules generate feedforward excitation and mutual inhibition, generating a set of motor sequence with flexibility in their transitions (Croll, 1975; Kawano et al., 2011; Piggott et al., 2011; Pirri and Alkema, 2012; Pirri et al., 2009; Wakabayashi et al., 2004; Wang et al., 2020).

Regulation of the turning amplitude and frequency of the Ω turn determines the effectiveness of escape. This involves neurons of and outside of the core escape circuit. With reduced food signals, a gustatory sensory neuron (ASI) and an interneuron (AIY) reduce the frequency of the Ω turn (Gray et al., 2005). Activation of AIB during long reversals increases turning frequency (Gordus

et al., 2015; Wang et al., 2020). The amplitude of Ω turn is coded by the excitatory head motor neurons (SMDs), and the ventral turning bias of Ω turn is specified by the motor neurons for ventral neck muscles (RIVs; Gray et al., 2005). Strong activation of an interneuron (RIM) inhibits head movements (Alkema et al., 2005; Pirri and Alkema, 2012; Pirri et al., 2009) during long reversals but facilitates body bending (Donnelly et al., 2013; Kagawa-Nagamura et al., 2018) after the animal initiates the Ω turn. Essential neuronal signaling for escape motor sequences has mostly focused on chemical and electrical signaling. These pioneering works significantly promote the escape "hard-wired" circuit.

Neuromodulation modifies properties and states of neurons and their connections (Grillner and Jessell, 2009; Marder et al., 2014). Modulators include a small number of monoamines and a large repertoire of peptides. Neuropeptides exhibit structural diversity, with astonishing functional specificity for neurons and circuit configurations (Grillner and Jessell, 2009; Marder and Bucher, 2001). An exemplary example is the crustacean stomatogastric ganglion, where over 50 neuropeptides act on a small set of neurons and synapses to produce different rhythmic output patterns (Blitz and Nusbaum, 2008; Ye et al., 2013). The *C. elegans* genome may encode up to 250 neuropeptides, which activate G-protein-coupled receptors (GPCRs) to initiate intracellular signaling cascades that exert long-lasting and long-range effects (Nassel, 2009). Several neuropeptides have been found to affect locomotion (Bhardwaj et al., 2018; Hu et al., 2011; Janssen et al., 2008; Lim et al., 2016; Meelkop et al., 2012; Oranth et al., 2018). However, neuropeptides or receptors that are directly involved in execution or regulation of escape have not been reported.

Combining behavioral studies, Ca^{2+} imaging, heterogeneous reconstitution, and *in situ* neuronal activity recordings, we identified the peptide NLP-18 and its receptor CKR-1, a $G\alpha_q$-protein-coupled receptor, to form an essential signaling pathway for Ω turn. We show that, through NLP-CKR-1 signaling pathway, the gustatory neuron (ASI) activates the interneuron (AIB)-to-motor neuron (SMD) subcircuit to allow Ω turn. Like synaptic transmission, this neuromodulatory signaling plays a selective and necessary role in an innate and robust motor action.

RESULTS

Escape steering requires peptidergic signaling

To examine the circuit underpinning escape steering, we first adapted an escape assay (Li et al., 2011) that robustly induces stereotype responses to afford easy quantification of turning. Using a platinum wire to deliver a single head touch per adult animal cultured on a thin layer of food (STAR Methods), 97% of wild-type (N2) animals evoked a three-step motor response: reversal; turn; and forward with a different heading angle (Figures 1A and 1B; Video S1). Among them, 76.3% ± 3.3% exhibited robust escape steering, defined by connecting reversal and forward movement with a head reorientation called a full Ω turn: the head bends; touches; and glides off the posterior half of the ventral body. Also, 21.0% ± 3.4% exhibited less robust head reorientation, connecting reversal and forward movement with a shallow Ω turn, where the head bends toward, but does not touch, the body (Figures 1A and 1D). A very small fraction of animals (2.7% ± 0.4%) exhibited no turn (no Ω), and even more rarely (2 in total 189 assays), they did a δ-shaped turn, where the head bends, touches the anterior body, and crosses over to exit at the dorsal body (Broekmans et al., 2016). Propensity and properties of turns are presented by three parameters: fraction of full versus shallow Ω turns; peak curvature of anterior body during turning (*entry* curvature); and angle of deepest middle body bending at the end of turning (exit angle; STAR Methods). This assay led to reliable responses (≥3 trials, at least 30 animals each trial).

To assess a potential involvement of peptidergic signaling, we compared escape steering of wild-type animals to mutant animals that cannot synthesize active neuropeptides. Active neuropeptides are derived from precursor proteins processed by a pro-protein convertase (PC) EGL-3 and a carboxypeptidase E (CPE) (EGL-21; Jacob and Kaplan, 2003; Kass et al., 2001). In the absence of either processing enzyme, propensity of full Ω turns was reduced to 23.0% ± 8% (*egl-3*; $p < 0.001$ against N2) and 16.7% ± 3% (*egl-21*; $p < 0.001$ against N2), respectively (Figures 1B and S1A). CAPS/UNC-31 is required for dense-core vesicle fusion and hence neuropeptide release. In the absence of CAPS, propensity of full Ω turn was similarly decreased (*unc-31* 27.7% ± 4.9%; $p < 0.001$ against N2). During escape, propensity of full Ω turns is positively correlated to the length of reversal (Zhao et al., 2003). Reduced proportion Ω turn in peptidergic signaling mutants may be consequential to a reduced reversal length. However, our assay induced a slightly increased reversal length between wild-type animals and animals that cannot synthesize active neuropeptides (*egl-3* 2.87 ± 0.14 mm, N2 2.25 ± 0.08 mm; $p < 0.001$; Figure 1E).

The *C. elegans* genome encodes three peptide families: the FMRF-amide-related (FLP); insulin-like (INS); and non-insulin/non-FMRF-amide-related but neuropeptide-like protein (NLP) (Husson and Schoofs, 2007; Li and Kim, 2008, 2010; Pierce et al., 2001), most of which require PC/EGL-3 processing. Insulin-like peptides function through an INS-family receptor (DAF-2) and a FOXO transcription factor (DAF-16). Reducing insulin-like signaling by either functional reduction of DAF-2 or elimination of DAF-16 did not alter propensity of full Ω turn during escape steering (Figure S1A).

Collectively, these results implicate a critical and specific requirement of non-ILP neuropeptides signaling underlying robust escape steering.

NLP-18 is critical for robust escape steering

We screened loss-of-function mutants for 20 FLP- and 12 NLP-encoding genes using our assay. Four exhibited statistically significant reduction of escape responses with full Ω turns. Among them, removal of an NLP encoding gene, *nlp-18*, led to the most consistent and closest degree of reduction (*nlp-18* 32.8% ± 1.4%; $p < 0.01$ against N2) to the effect of removing EGL-3 (Figure S1B). Removal of three FLP-encoding genes also reduced the propensity of full Ω turns, but their effect was either modest (*flp-18* and *flp-20*) or inconsistent between trials (*flp-1*; Figure S1C).

The *nlp-18* gene (Figure 2A) encodes a propeptide, which is processed into five mature peptides called NLP-18a–e, respectively (Figure 2B). *nlp-18*(*ok1557*) is a null allele that removes the

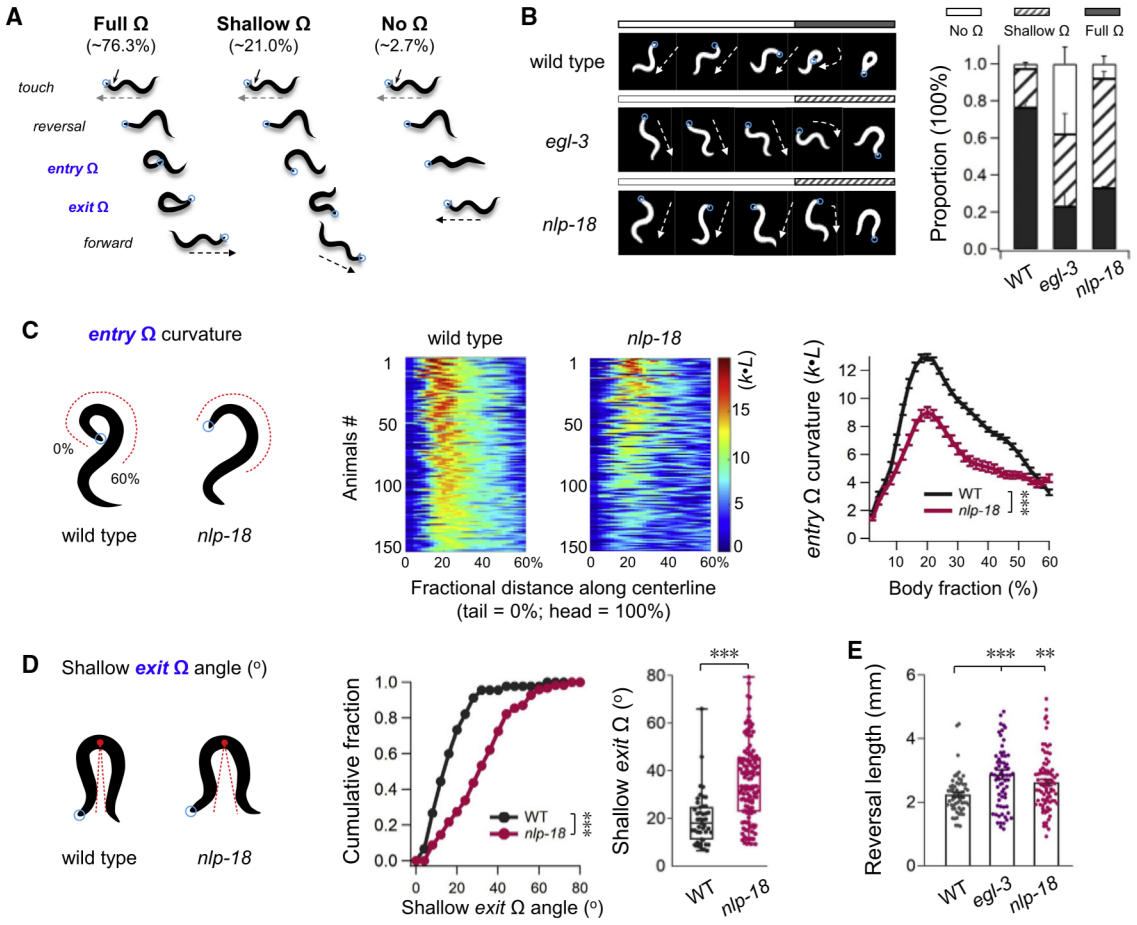

Figure 1. Mutant in neuropeptide-like peptide gene *nlp-18* disrupted the robustness of Omega turn

(A) A sketch diagram of escape response by head touch, including reversal, omega (Ω) turn, and following forward movement. Blue circles denote the head; dash arrows denote the forward orientation.

(B) Sequential snapshots of representative Ω body postures and quantification of the full Ω proportion in different genotypes. Mutants in *egl-3* and *nlp-18* display obvious Ω turn defects, and shallower Ωs were mostly observed (n ≥ 5 trials, at least 30 animals each trial). Proportion analysis with the Fisher's exact test. WT, wild type.

(C) (Left) Schematic representation of the entry Ω curvature. (Right) Representative color maps and average curvatures of the entry Ω in wild-type and *nlp-18* mutant animals (n ≥ 150 animals) are shown. ***p < 0.001; two-way ANOVA test.

(D) (Left) Schematic representation of the shallow exit Ω angle. The exit Ω angle was defined as the angle from the deepest point in the bend to the closest points anterior and posterior of the animal. (Right) The distribution and quantification of all shallow exit Ω angles in wild-type and *nlp-18* mutant animals, respectively, are shown (n ≥ 45 animals). ***p < 0.001; Kolmogorov-Smirnov test (left) and Mann-Whitney test (right).

(E) Harsh touch induced reversal length in different genotypes (n ≥ 60 animals). **p < 0.01; ***p < 0.001; Mann-Whitney test.

All data are expressed as mean ± SEM.

partial propeptide coding sequence (Figure 2A). *nlp-18*-null mutants entered the turn with significantly reduced curvature than wild-type animals (Figure 1C). Not only had a much higher proportion of *nlp-18* mutant animals exited with a shallow Ω turn (~60%) than wild-type animals (~20%; Figure 1B), shallow Ω turns occurred at a higher exit angle for *nlp-18* mutants than wild-type animals (Figure 1D; Video S2). Similar to *egl-3* mutants, duration of reversal in *nlp-18* mutants was slightly increased during evoked escape (2.62 ± 0.09 mm versus 2.25 ± 0.08 mm for N2 wild type; $p < 0.01$; Figure 1E). Spontaneous velocity and propensity of directional movement were unchanged in *nlp-18* mutants (Figures S3A and S3B). These results demonstrate that *nlp-18* may specifically promote a full Ω turn.

Requirement of *nlp-18* for robust escape steering is not unique to mechanical stimuli. When we evoked escape by either an aversive metal (Figure S1D) or high osmolarity (Figure S1E), removal of *nlp-18* led to reduced propensity for full Ω turn and increased propensity for shallow Ω turn, as well as shallow Ω turns with reduced entry curvature and increased exit angles. Thus, *nlp-18* is an inherent component of the escape circuit to promote deep turning.

NLP-18 promotes escape steering mainly from the ASI sensory neuron

To pinpoint NLP-18's role in the escape circuit, we first assessed its cellular origin. A transcriptional reporter for *nlp-18* (STAR

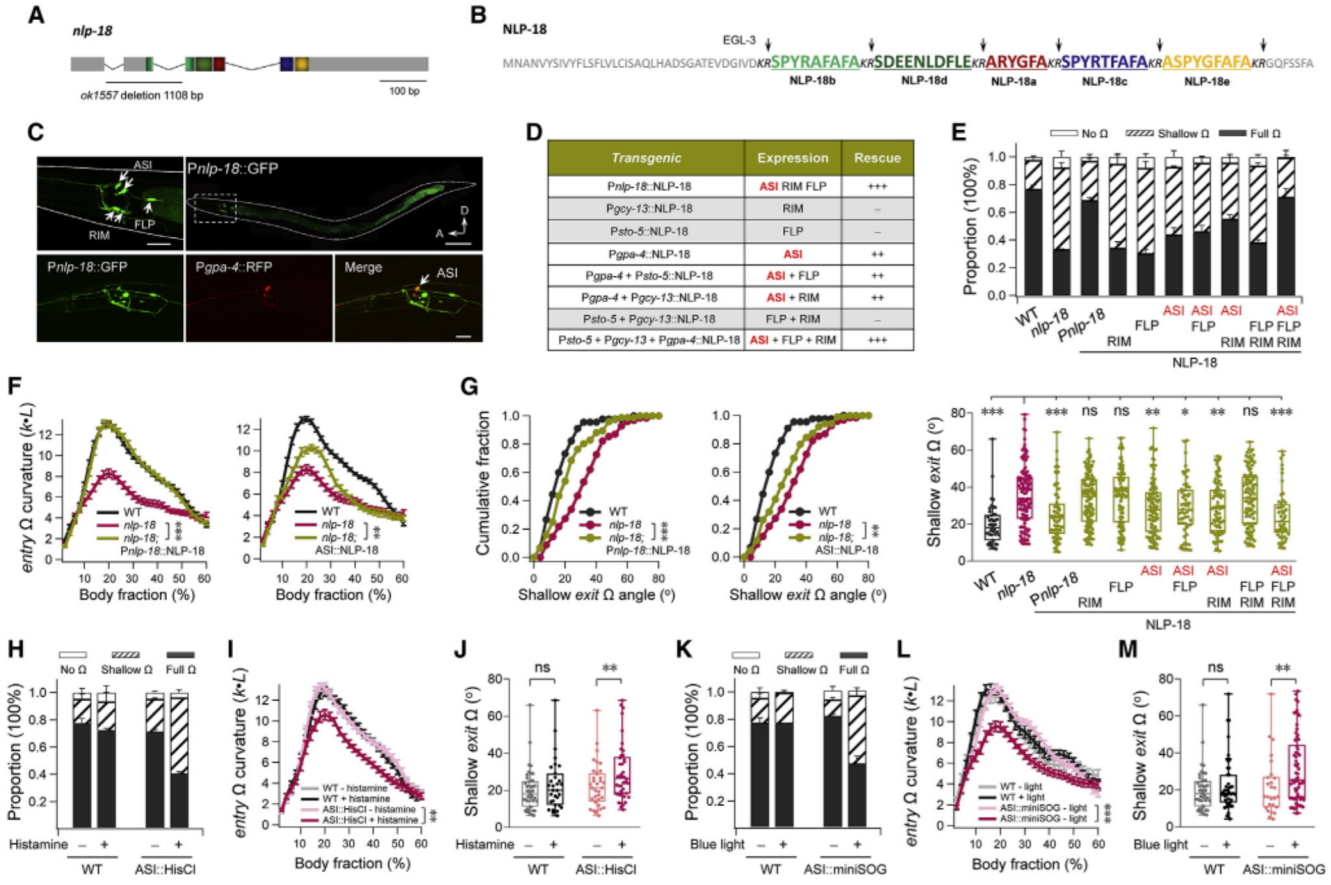

Figure 2. ASI neurons are critical for *nlp-18*-modulated robust escape steering

(A) The gene structure of *nlp-18*(*ok1557*) with 1,108 bp deletion indication.

(B) *nlp-18* encodes a neuropeptide precursor that harbors five putative neuropeptides, which are flanked by the dibasic *KR* (arrow) cleaving sites. Colors label the predicted neuropeptide sequences (red NLP-18a, green NLP-18b, blue NLP-18c, dark green NLP-18d, and golden NLP-18e).

(C) Expression pattern of *nlp-18*. Top: endogenous *nlp-18*-promoter-driven GFP was observed in three head neurons (ASI, FLP, and RIM) and intestine. Scale bars, left 20 μm and right 100 μm. Bottom: the co-localization of P*nlp-18*:GFP and P*gpa-4*:RFP in ASI neurons is shown. Scale bar, 20 μm. Worm orientation: A, anterior; D, dorsal.

(D) Summary of the rescue of Ω turn deficiency by the expression of NLP-18 in different neurons. –, no rescue; +, slight rescue; ++, moderate rescue; +++, full rescue.

(E) Propensity of the head-touch-induced escape responses (no Ω, shallow Ω, and full Ω) from wild-type, *nlp-18*, and the rescue strains ($n \geq 150$ animals). Proportion analysis with the Fisher's exact test is shown.

(F and G) The entry Ω curvature and shallow exit Ω angle were restored by self-promoter-driven NLP-18 and ASI-specific expression of NLP-18 ($n \geq 45$ animals). Two-way ANOVA tested in (F) and Kolmogorov-Smirnov test in (G) (left). $^{**}p < 0.01$ and $^{***}p < 0.001$. ns, not significant.

(H–J) Silence of ASI neurons by histamine (10 mM) significantly reduced the full Ω proportion (H) and the entry Ω curvature (I) and increased the shallow exit Ω angle (J). Fisher's exact test in (H); two-way ANOVA tested in (I), $^{**}p < 0.01$; Mann-Whitney test in (J), $^{**}p < 0.01$.

(K–M) Ablation of ASI neurons significantly reduced the full Ω proportion (K) and the entry Ω curvature (L) and increased the shallow exit Ω angle (M). Fisher's exact test in (K); two-way ANOVA tested in (L), $^{***}p < 0.001$; Mann-Whitney test in (M), $^{**}p < 0.01$.

(H–M) $n \geq 3$ trials, each with at least 30 worms tested. Data are presented as mean ± SEM.

Methods) revealed strong expression in the intestine and three pairs of neurons: a gustatory sensory neuron (ASI); a mechanical sensory neuron (FLP); and an interneuron (RIM; Figures 2C and S2B). When NLP-18 expression was restored by this promoter, *nlp-18* mutants' turning defects were fully rescued (Figures 2D, S2C, and S2D). This result implicates functional sufficiency of *nlp-18* among these cells.

We then systematically tested the functional requirement for individual cells using exogenous promoters. Driving NLP-18 expression in the intestine did not change escape behaviors of *nlp-18* mutants (data not shown). Expression of NLP-18 in the mechanosensory neuron (FLP) or interneuron (RIM) did not rescue *nlp-18* mutants either. By contrast, driving NLP-18 expression in the gustatory sensory neuron (ASI) significantly rescued *nlp-18* mutant animal's turning defects in our assay, with an increased propensity of full Ω turns (Figures 2D and 2E), increased entry body curvature of the turn (Figure 2F), and decreased exit angles at the end of shallow Ω turns (Figure 2G). Restoring NLP-18 in three neurons together led to an effect qualitatively similar to that of ASI-specific NLP-18 expression,

with modest but statistically significant improvement (Figures 2E–2G).

Implication of this result—NLP-18 promotes robust escape steering from the ASI neurons—surprised us. A previous laser ablation study found that ASIs inhibit the frequency of short reversals and Ω turns in a food-signal-dependent manner (Gray et al., 2005). To clarify the role of ASI during escape steering, we examined the effect of silencing ASI neurons using histamine-gated chloride channel (HisCl) (Pokala et al., 2014). Exposure of animals that ectopically and specifically expressed HisCl in ASI to histamine led to reduced full Ω turns and increased shallow Ω turns (Figure 2H), as well as reduced entry curvature and larger exit angle for shallow Ω turns (Figures 2I and 2G). We observed similar effects (Figures 2K–2M) when we ablated ASI using mini-singlet oxygen generator (miniSOG) (Qi et al., 2012; Shu et al., 2011). *nlp-18* mutant's escape steering defect was also not affected by the absence of food (Figures S3E–S3G). These results confirm that the gustatory sensory neurons ASIs are required for NLP-18-dependent robust escape steering.

A cholecystokinin receptor CKR-1 promotes robust escape steering

Molecular mapping of receptors is necessary to delineate peptidergic signaling. To identify NLP-18's physiological receptors, we started by examining deletion mutants for GPCRs using our assay. Approximately 150 predicted *C. elegans* GPCRs have significant sequence homologies to peptidergic receptors in other systems (Frooninckx et al., 2012; Janssen et al., 2010). Among them, we screened 31 with significant homology to mammalian peptidergic receptors, including the cholecystokinin receptor (CKR), neuropeptide receptor (NPR), and neuromedin U receptor (NMUR) families, as well as receptors predicted to bind NLPs (Frooninckx et al., 2012).

Among them, removal of the *ckr-1* gene led to severely reduced escape steering (Figure S3C). CKR-1 is closely related in sequence to the CKR CCKR-1/CCKAR (Figures 3A, 3B, and S3D), receptors implicating satiety, anxiety, and gall bladder contraction (Berna et al., 2007). *ckr-1* mutant animals' escape defects are highly reminiscent to *nlp-18* mutants, with reduced full Ω turn propensity (Figure 3C), increased entry curvature (Figure 3D), and reduced exit angle (Figure 3E). Compared with *nlp-18* mutants, the severity of *ckr-1*'s defect was slightly reduced. Reversal length during evoked escape was not altered in *ckr-1* mutants (2.22 ± 0.09 mm versus N2 2.25 ± 0.08 mm; $p > 0.05$; Figure 3F). Spontaneous velocity and partition between directional movements were also unchanged in *ckr-1*, *nlp-18*, or *nlp-18*; *ckr-1* mutants (Figures S3A and S3B). Similar to *nlp-18* mutants, *ckr-1*'s steering defect is not dependent on food signals (Figures S3E–S3G).

These results indicate that CKR-1 and NLP-18 function in the same signaling pathway to promote robust escape steering.

Ckr-1 promotes steering from the motor (SMD) and interneurons (AIB) of the escape circuit

To map where NLP-18-CKR-1-signaling pathway may take place, we first sought where CKR-1 resides in the escape circuit. A functional transcriptional reporter for CKR-1 revealed strong expression in many neurons and weak expression in the intestine (Figure 4A). CKR-1-expressing neurons include head motor neurons SMD and RME (Figure 4B), interneurons AIB and RIM, peptidergic neurons RIS, and body motor neurons A, B, and D. All are involved in motor behaviors. Among them, SMD, RME, AIB, and RIM have been implicated in motor sequences specific for escape (Alkema et al., 2005; Gray et al., 2005; Hendricks et al., 2012; Kaplan et al., 2020; Pirri et al., 2009; Shen et al., 2016; Wang et al., 2020).

We identified key neurons through which CKR-1 promotes escape steering by restoration of its expression using exogenous promoters that overlap with those cells. Driving CKR-1 expression in either SMD (by P*flp-22*, P*ntr-2*, or P*glr-1*) or AIB (by P*aptf-1* or P*npr-9*) led to a robust rescue of escape steering defects in *ckr-1* mutant animals (Figure 4C), evaluated by the proportion of full Ω turns (Figure 4D), entry curvature (Figure 4E), and exit angle (Figure 4F). Driving CKR-1 expression in all other neurons or the intestine did not lead to rescue (Figures 4C, 4D, 4F, S4A, and S4B).

Restoring CKR-1 in either SMD or AIB led to near full degree of rescue, which implicates redundancy of CKR-1 signaling in the escape circuit. Alternatively, it may be an artifact of exogenously restored expression, because exogenous promoters did not deliver CKR-1 at its physiological level and, in some experiments, introduced ectopic CKR-1 signaling in the circuit. To further verify where endogenous CKR-1 functions from, we examined the effect of depletion of CKR-1 protein from SMD or AIB, using a repurposed non-neuronal ubiquitin system (Armenti et al., 2014). Briefly, we tagged the endogenous *ckr-1* locus with ZF1, an E3-recognition target signal for the ZIF-1 ligase. When ZIF-1 is expressed in targeted neurons, endogenous CKR-1 proteins are degraded cell specifically (STAR Methods).

Insertion of the ZF1 motif into the *ckr-1* locus did not change behaviors (Figure 4G), development, or physiology. When ZIF-1 was expressed in either SMD or AIB neurons in *ckr-1*:ZF1 animals (GB01), they exhibited less robust escape steering, where turning included less full Ω turns, the entry curvature when starting the turn was decreased, whereas the exit angle was significantly increased (Figures 4G–4I). The defect in escape behavior of these animals qualitatively resembles that of *ckr-1* genetic deletion mutant. Critically, results of the rescue and mimic experiments corroborate that CKR-1-mediated signaling can promote deep turning through either the AIB interneuron or the SMD head motor neuron.

CKR-1 encodes a $G\alpha_q$-protein-coupled receptor

CKR-1's mammalian homologue CCKR-1 is a G-protein-coupled receptor. *C. elegans* has homologs for four mammalian Gα subtypes, EGL-30/$G\alpha_q$, GSA-1/$G\alpha_s$, GOA-1/$G\alpha_{i/o}$, and GPA-12/$G\alpha_{12/13}$ (Frooninckx et al., 2012; Jansen et al., 1999). EGL-30 binds and activates EGL-8, the PLCβ homolog, which converts phosphatidylinositol 4,5-bisphosphate (PIP_2) to DAG and inositol triphosphate (IP_3) to initiate endoplasmic reticulum (ER) Ca^{2+} release. Among four Gα subtypes, only EGL-30/$G\alpha_q$ is required for the full Ω proportion (Figure 5A). Full Ω proportion was also reduced in *egl-8* mutant, to the same level of *egl-30*. Entry Ω curvature, as well as the shallow exit Ω angle, was significantly reduced in *egl-8* mutant, supporting that $G\alpha_q$ signaling is required for the escape steering. Importantly, removing CKR-1 in *egl-30* or *egl-8* mutant did not further enhance their escape defects (Figures 5B, 5D, and 5E), further supporting that *ckr-1* and

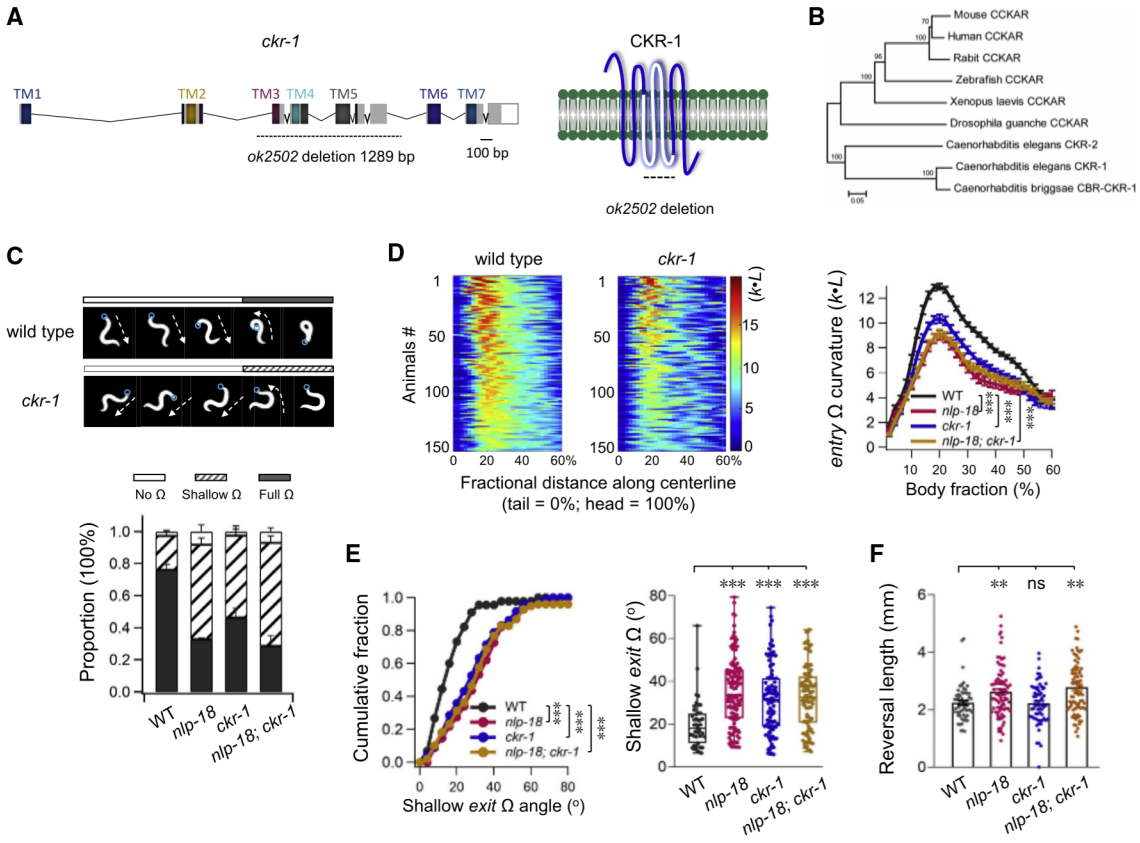

Figure 3. CKR-1, a cholecystokinin receptor, is required for robust escape steering

(A) The gene and protein structure of *ckr-1(ok2502)* with 1,289 bp deletion indication. Seven predicted transmembrane (TM) domains were marked.

(B) Phylogenetic tree (analyzed by MEGA 6.60) demonstrates that *C. elegans ckr-1* encodes a cholecystokinin A receptor.

(C) (Top) Sequential snapshots of representative body postures of the Ω turn in wild type and *ckr-1*. Blue points denote the head. (Bottom) Propensity of head-touch-evoked escape responses (no Ω, shallow Ω, and full Ω) in wild type, *nlp-18*, *ckr-1*, and *nlp-18*; *ckr-1* double mutants is shown (≥5 trials, at least 30 animals each trial). Fisher's exact test in (C) (bottom).

(D) Representative color maps and quantification of the entry Ω curvature in wild type, *ckr-1*, and *nlp-18*; *ckr-1* mutants (n ≥ 150 animals). ***p < 0.001; two-way ANOVA test.

(E) *ckr-1* and *nlp-18*; *ckr-1* show similar increased shallow exit Ω angle phenotype of *nlp-18* (n ≥ 45 animals). Kolmogorov-Smirnov test (left); Mann-Whitney test (right). ***p < 0.001.

(F) Harsh-touch-induced reversal length in different genotypes (n ≥ 60 animals). Mann-Whitney test, **p < 0.01.

Data are expressed as mean ± SEM.

egl-30, *egl-8* are in the same signaling pathway. Thus, CKR-1 functions as a $G\alpha_q$-coupled receptor to regulate escape steering (Figure 5C).

SMD motor neurons exhibit NLP-18-CKR-1-dependent activity increase during the Ω turn

Two neurons we found to be involved in CKR-1 signaling play different roles in *C. elegans* motor behaviors. AIB's Ca^{2+} dynamics correlate with the transition between reversal and turning (Wang et al., 2020), whereas SMD's periodic Ca^{2+} undulation correlate with ventral and dorsal head bends (Hendricks et al., 2012; Kaplan et al., 2020).

We measured the SMD activity in freely moving animals by a genetic calcium sensor GCaMP6s (STAR Methods). As reported in above studies, SMDV and SMDD exhibited calcium signals that correlate with ventral and dorsal head bending during foraging and turning. Animals turn both ventrally and dorsally. Here, we focused on activity of SMDD neurons and their correlation with dorsal turns (Figure 6A). When evoked to escape, SMDD exhibited periodic Ca^{2+} dynamics (peak value denoted as R Ca^{2+}; Figure 6B), which positively correlated with the dorsal head bending (Figures 6B and 6C). After the movement transited into a full Ω turn, we noticed a further increase of Ca^{2+} signals (peak value denoted as Ω Ca^{2+}; Figure 6B; Video S3). The further increase of Ω Ca^{2+} from R Ca^{2+} was significant (Figure 6D) and expected: a deeper head bend during the Ω turn reflects higher SMD activity and increased excitatory inputs to head muscles.

In *nlp-18* or *ckr-1* mutants, SMDD continued to exhibit oscillatory Ca^{2+} signals during reversal and turns similar to wild-type animals (Figures S5A and S5B). We found that the removal of *nlp-18* or *ckr-1* does not alter SMDD's R Ca^{2+} peak and dynamics (Figures S5C–S5E). We also did not observe elevation of R Ca^{2+}

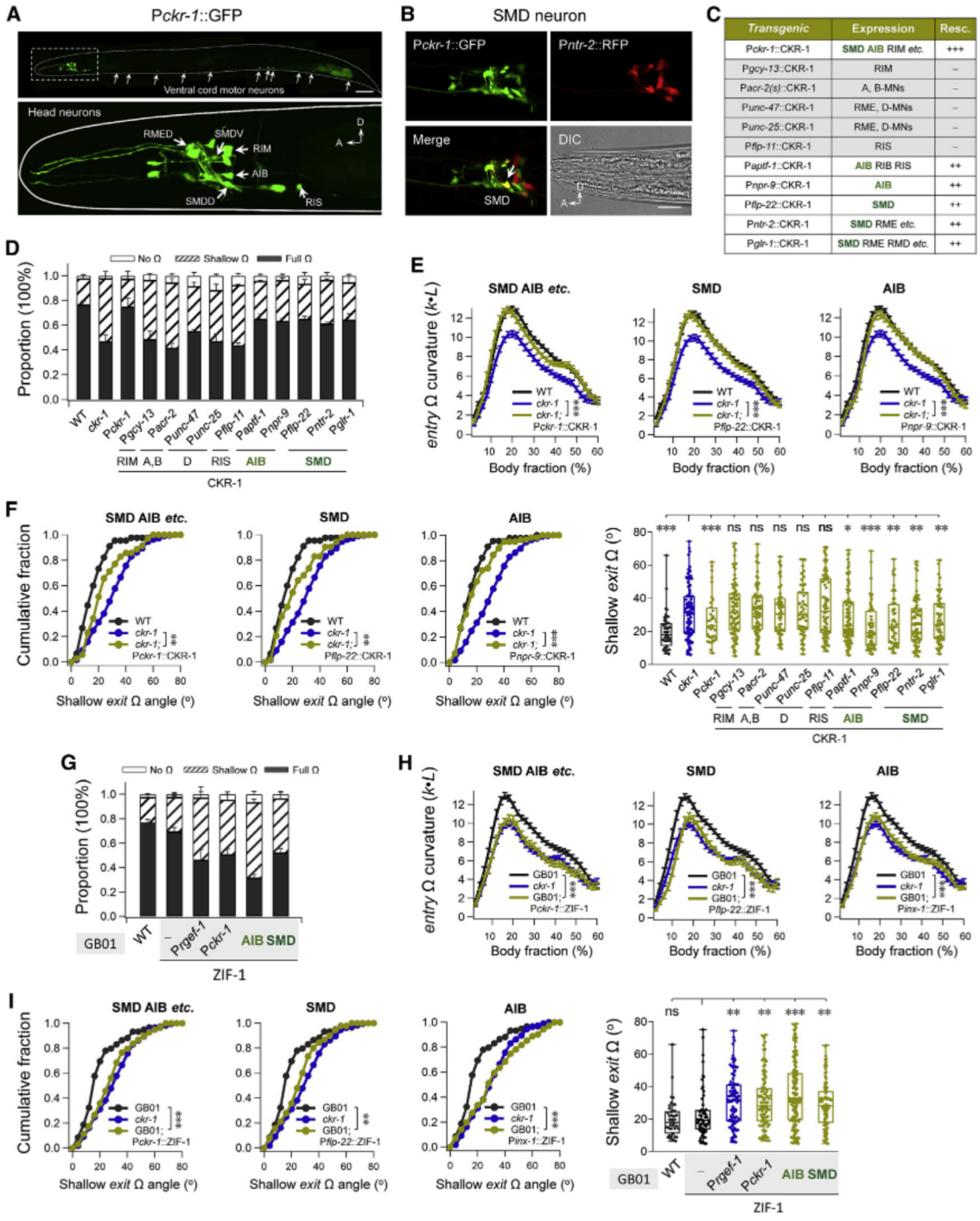

Figure 4. CKR-1 regulates escape steering robustness from SMD/AIB neurons

(A) Expression pattern of *ckr-1*. Top: *ckr-1* expresses in the *C. elegans* nervous system, including the head and ventral cord neurons. The boxed-in area shows the head neurons that are presented in the bottom panel. The arrows denote the expression of *ckr-1* in ventral cord motor neurons. Scale bar, 100 μm. Bottom: representative head neurons are shown.

(B) The P*ckr-1*:GFP expression in SMD neurons; scale bar, 20 μm.

(C) Summary of the rescue potency of Ω turn deficiency expression of CKR-1 in different neurons, from which SMD and AIB exhibit critical functions of *ckr-1*. –, no rescue; +, slight rescue; ++, moderate rescue; +++, full rescue.

(legend continued on next page)

elevation, even when animals performed shallow turning (Figures 6D, S5A, and S5B; Video S4). Consistent with the non-additive steering defects exhibited by *nlp-18*; *ckr-1* double-mutant animals, SMD neurons exhibited a similar degree of reduction of turning-related elevation to either single-mutant animal. In *nlp-18* mutant animals, expression of NLP-18 in ASI neurons restored Ω Ca^{2+} (Figures 6D and 6E). In *ckr-1* mutant animals, expression of CKR-1 in SMD also restored Ω Ca^{2+} (Figures 6D and 6E). Together, NLP-18-CKR-1 signaling promotes the Ω turn.

CKR-1 is a receptor of NLP-18

Our functional data propose that NLP-18 and CKR-1 activate $G\alpha_q$ signaling to promote robust escape steering. We investigate whether this effect is direct: CKR-1 as a receptor of NLP-18.

First, we tested the hypothesis in the heterologous *X. laevis* oocyte system. Synthetic NLP-18 did not elicit endogenous currents in control oocytes (Figure 7A, empty vector). When *ckr-1* cRNA was injected in the oocyte, synthetic NLP-18 (NLP-18a–NLP-18e) evoked robust currents (Figures 7A and 7B). There are five predicted NLP-18 peptides, four with the hallmark C-terminal residues for the NLP peptides "FAFA" (NLP-18b, c, and e) or "FA" (NLP-18a) (Figure 7A) and one without (NLP-18d). While all evoked currents, those with the FA motif were more potent (Figure 7B). Indeed, truncation of the FAFA residues from NLP-18c (NLP-18cΔ) led to a significantly reduced current (data not shown), predicting a necessary motif for high-affinity binding. Application of five NLP-18 neuropeptides together (1 μM of each) activated only slightly larger current than single peptides, indicating activation saturation (Figures 7A and 7B). Under this condition, the half-effect concentration (EC_{50}) of NLP-18a was ~13 nM (Figure 7C), within the range for cognate receptor activation (Rogers et al., 2003).

Next, we asked whether NLP-18 could activate endogenous CKR-1 in *C. elegans* neurons. We applied a *C. elegans* dissection preparation to expose SMD motor neurons that expressed GCaMP6s (Figure 6) and assessed their calcium dynamics evoked by synthesized NLP-18 (NLP-18a-e mix; see STAR Methods). Application of synthetic NLP-18 evoked ~30% increase at peak Ca^{2+} signals (Figure 7D). Evoked Ca^{2+} increase was abolished in *ckr-1* mutant animals and were partially restored by CKR-1 expression in SMD (Figure 7D). Consistent with CKR-1 encoding a $G\alpha_q$-protein-coupled receptor, NLP-18-evoked Ca^{2+} increase in SMD was also abolished in *egl-30* and *egl-8* mutant animals (Figure 7F). In *ckr-1*; *egl-30* and *ckr-1*; *egl-8* double mutants, the Ca^{2+} transient increase was reduced to the same level in *egl-30* and *egl-8* single mutants, respectively. In the *ckr-1*; *egl-8* mutant, restoring CKR-1 expression in SMD could not rescue the Ca^{2+} increase (Figure 7F). We conclude that CKR-1 functions as a direct receptor of NLP-18 to increase SMD motor neuron's activity by $G\alpha_q$ signaling.

AIB functions mainly through SMD

During escape, the rise and fall of AIB activity transits the animal from reversal to turn (Wang et al., 2020), which is led by a deep head bend driven by SMD (Gray et al., 2005; Kaplan et al., 2020). Expression of CKR-1 in AIB robustly rescued *ckr-1* mutant animal's escape defects (Figure 4C). We found that restoring CKR-1 in AIB also rescued SMD's Ca^{2+} increase (Figure 7D) but with an extended delay (latency 4.3 ± 0.5 s) when compared with restoring CKR-1 in SMD (latency 1.1 ± 0.3 s; $p < 0.001$) or wild-type animals (latency 1.4 ± 0.3 s; $p < 0.001$; Figure 7E). This is consistent with AIB functioning at the upper circuit layer to activate turning (Gray et al., 2005).

The observation that restoring *ckr-1* expression in the *ckr-1*-expressing interneurons, such as RIM (P*gcy-13*:CKR-1), of mutant animals was not able to restore escape defects or SMD's calcium increase suggests that NLP-18-CKR-1 signaling may function through hard-wired circuit connections (Figure 7D). Indeed, upon ablation of SMD neurons by miniSOG, expression of CKR-1 in AIB severely reverted its rescuing effect in escape steering (Figure S6). Interestingly, they maintained some capacity of full escape steering (Figure S6), suggesting that AIB may function through a minor, secondary pathway to promote turning.

In summary, we show here that NLP-18, released mainly from the ASI sensory neurons, activates the CKR-1 GPCR in the SMD head motor neurons and AIB interneurons to strengthen escape steering (Figures 7G and 7H). The NLP-18-CKR-1-signaling pathway is an integral component of the escape response.

DISCUSSION

With increasingly detailed understanding of the molecular and cellular composition of *C. elegans* wiring (Bargmann, 1998; Cook et al., 2019; Taylor et al., 2021; White et al., 1986; Witvliet et al., 2021), it is possible to functionally dissect the role of neuropeptidergic signaling at single-neuron resolution. *C. elegans* generates innate motor response to escape noxious stimuli through dedicated neural circuit. We discover a peptidergic (NLP-18)-GPCR (CKR-1)-signaling pathway as a necessary component of the innate escape steering. Instead of a slow and lasting modulation of a circuit state, this signaling event functions selectively and temporally to enable reorientation steering, the Ω turn.

(D) Distribution of the head-touch-induced escape responses (no Ω, shallow Ω, and full Ω) in distinct transgenic strains ($n \geq 5$ trials, at least 30 animals each trial). Proportion analysis with the Fisher's exact test is shown.

(E and F) The entry Ω curvature and shallow exit Ω angle in *ckr-1* mutant were rescued by the expression of CKR-1 in SMD and AIB neurons ($n \geq 45$ animals). Two-way ANOVA test was used in (E). Shallow exit Ω angle cumulative fraction was tested by Kolmogorov-Smirnov in (F) (left) and Mann-Whitney test in (F) (right). *$p < 0.05$, **$p < 0.01$, and ***$p < 0.001$.

(G) Composition of the head-touch-induced escape responses (no Ω, shallow Ω, and full Ω) in wild-type, *ckr-1*, and CKR-1 knockdown strains with the expression of neuronal specific ZIF-1 in GB01 *gaals1* background (≥5 trials, at least 30 animals each trial). Proportion analysis with the Fisher's exact test is shown.

(H and I) The entry Ω curvature and shallow exit Ω angle in GB01 were reduced by the expression of ZIF-1 in SMD and AIB neurons. (I) Scatter diagram and quantification of the shallow exit Ω angles from different knockdown strains ($n \geq 46$ animals). Two-way ANOVA test in (H). Shallow exit Ω angle cumulative fraction was tested by Kolmogorov-Smirnov in (I) (left) and Mann-Whitney in (I) (right). **$p < 0.01$ and ***$p < 0.001$.

Data are expressed as mean ± SEM.

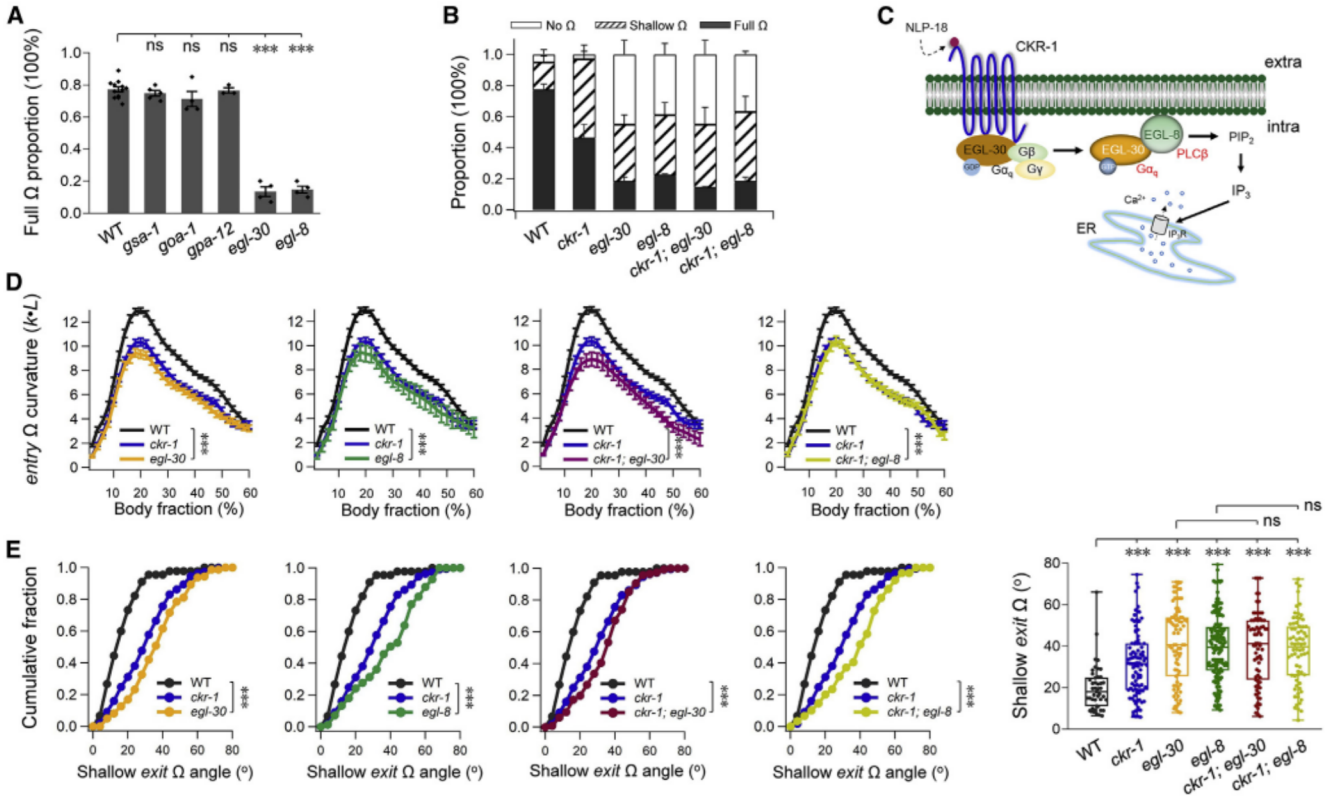

Figure 5. CKR-1 is a Gα_q -protein-coupled receptor

(A) Quantification of the full Ω proportion in wild type and various G-protein-signaling mutants. The full Ω proportion was specifically reduced in *egl-30* and *egl-8* mutants. ***p < 0.001; Student's t test.

(B) Composition of the head-touch-induced escape responses (no Ω, shallow Ω, and full Ω) in wild type, *ckr-1*, and respective mutants. *ckr-1* could not further reduce the full Ω proportion in *egl-30* and *egl-8* mutants.

(A and B) n ≥ 3 trials, at least 30 animals each trial. Proportion analysis with the Fisher's exact test is shown.

(C) Schematics of putative CKR-1 G-protein-coupling signaling pathway. CKR-1 is coupled by the Gα_q protein.

(D and E) The entry Ω curvature and shallow exit Ω angle recapitulate the level of *ckr-1* mutant in *egl-30*, *egl-8* single mutant, and *ckr-1*; *egl-30* and *ckr-1*; *egl-8* double mutants. *ckr-1* could not further reduce the shallow exit Ω angle in *egl-30* and *egl-8* mutant backgrounds (n ≥ 46 animals). Two-way ANOVA test was used to access the statistical difference in (D). Shallow exit Ω angle cumulative fraction was tested by Kolmogorov-Smirnov in (E) (left) and Mann-Whitney in (E) (right). ***p < 0.001.

Data are expressed as mean ± SEM.

A necessity of peptidergic signaling in innate behaviors

Shared characteristics of innate behaviors reflect shared properties of the underlying circuits. Across species, escape behaviors are instinctual, executed with speed and robustness. The fast forms of neural transmission, through electrical and excitatory synaptic transmissions in the reflexive escape motor response, have been shown in vertebrate like larval zebrafish (Dunn et al., 2016; Miller et al., 2017). Withdrawal, however, is only one motor step of the escape response. Previous and ongoing work in *C. elegans* is examining this response for not only other steps but also their transitions. This enables a systematic investigation and modeling of robust, but not rigid, behaviors at the molecular, cellular, and systems levels. To date, the fast neural transmissions within the circuits that drive escape behavior have been largely characterized (Chalfie et al., 1985; Gray et al., 2005; Pirri and Alkema, 2012; Wang et al., 2020).

Working in parallel with neurotransmitters, neuropeptides exert effects for innate behavior on relatively slow timescales through intracellular signaling cascades (Bargmann, 2012; Bargmann and Marder, 2013). For example, the neuropeptides hypocretin and orexin produced in hypothalamic neurons are crucial regulators of sleep and wakefulness (Sakurai, 2007). Here, we identified a peptidergic signaling pathway that underlies a motor behavior during escape. The NLP-18-CKR-1-signaling pathway specifically enhances escape steering, but not in other modalities, such as spontaneous velocity. This functional specificity of NLP-18 reflects spatial specificity by origin (ASI) and target neurons (AIB and SMD), as well as the temporal specificity by its activation of head motor neurons during turning. Such a mode of function differs from what is generally sought to be a slow, long-range, and long-lasting form of neuromodulation.

Functional conservation of GPCR receptors by sequence-divergent signaling peptides

CKR-1 exhibits high sequence homology to the vertebrate CCK1R (or CCKAR; Figures 3A, 3B, and S3D). Same as the

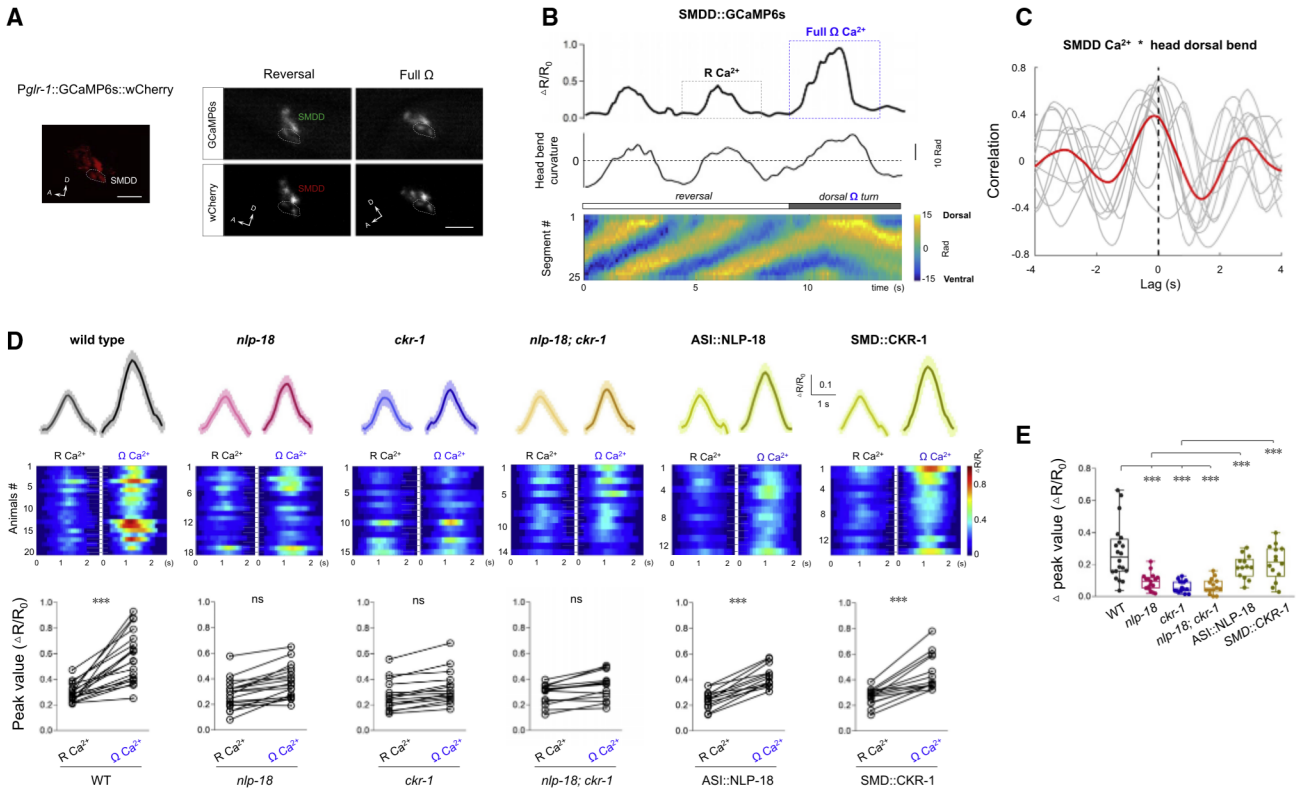

Figure 6. The Ω Ca^{2+} of SMD neurons was reduced in escape steering mutants

(A) Representative images showing fluorescence of GCaMP6s and wCherry in the SMDD soma of P*glr-1*:GCaMP6s:wCherry transgenic worms during reversal and full Ω. Left: a pair of SMDD:wCherry identified by 60× objective is shown. Scale bars, 10 μm.

(B) Top: representative Ca^{2+} transient trace of SMDD and head bend curvature in the process of reversal and turn from a free-behaving animal. △R/R0, normalized GCaMP/wCherry ratio. Bottom: posture kymograms are shown.

(C) Cross-correlation between SMDD Ca^{2+} and head dorsal bend. Faint lines indicate the results from individual animals, and the red line indicates mean value (n = 10 animals).

(D) Top: the average traces of the last R Ca^{2+} and Ω Ca^{2+} in different genotypes. Middle: the representative color maps of the corresponding Ca^{2+} activities are shown. Bottom: the peak Ca^{2+} values of the adjacent R Ca^{2+} and Ω Ca^{2+} in different genotypes are shown. ***p < 0.001; Wilcoxon matched-pairs signed rank test was used.

(E) Scatter diagram and quantification of the peak value difference between the R Ca^{2+} and Ω Ca^{2+}, which was abolished in *nlp-18*, *ckr-1*, and *nlp-18*; *ckr-1* mutants. Neuronal specific expression of NLP-18 in ASI in *nlp-18* and CKR-1 in SMD in *ckr-1* could restore the Ω Ca^{2+} (n ≥ 13 animals). ***p < 0.001; Mann-Whitney test.

Data are expressed as mean ± SEM.

human CCK1R (Dufresne et al., 2006), CKR-1 is a $G\alpha_q$-protein-coupled receptor (Figure 5). Human CCK1R is expressed in the gastrointestinal tract and discrete brain areas, coinciding with CKR-1's expression in *C. elegans* intestine and a selected group of sensory, motor, and interneurons. These similarities implicate potential common physiological contributions. Activation of CCK1R induces satiety, an innate feedback on food intake (Jensen, 2002), and disruption of human CCK1R causes psychiatric disorders (Shintaku et al., 1992). *C. elegans* NLP-18-CKR-1 signaling involves the gustatory sensory neuron and escape response. NLP-18's primary neuronal source, the ASI neurons, is known to secrete hormone-like peptides insulin and transforming growth factor β (TGF-β) (Pandey et al., 2021; You et al., 2008). There might be potential conservation of CKR-1's role in neural circuits.

Neuropeptides are generally considered to be species specific due to low primary sequence identity. Our investigation of CKR-1's physiological role led to its cognate ligand NLP-18, challenging this notion. There is no steering defect in loss of function of *ckr-2*, another putative CCKR homologue, supporting NLP-18's specificity for CKR-1. Known CCK1R ligands, CCK in vertebrate, gastrin in arthropod, and NLP-18 in *C. elegans*, do not exhibit strong sequence similarity. However, CCK was also found in the gastrointestinal tract (Ivy and Oldberg, 1928) and the brain (Beinfeld, 1983), bearing resemblance to NLP-18's presence in the intestine and sensory and interneurons. Both peptides show dose-dependent activation of the CKR receptor coupled with $G\alpha_q$ signaling. NLP-18 exhibits high affinity to CKR-1, with initiation activation at 1 nM and half-activation at 13 nM. CCK-8 was reported to activate CCKR1 between 1 nM

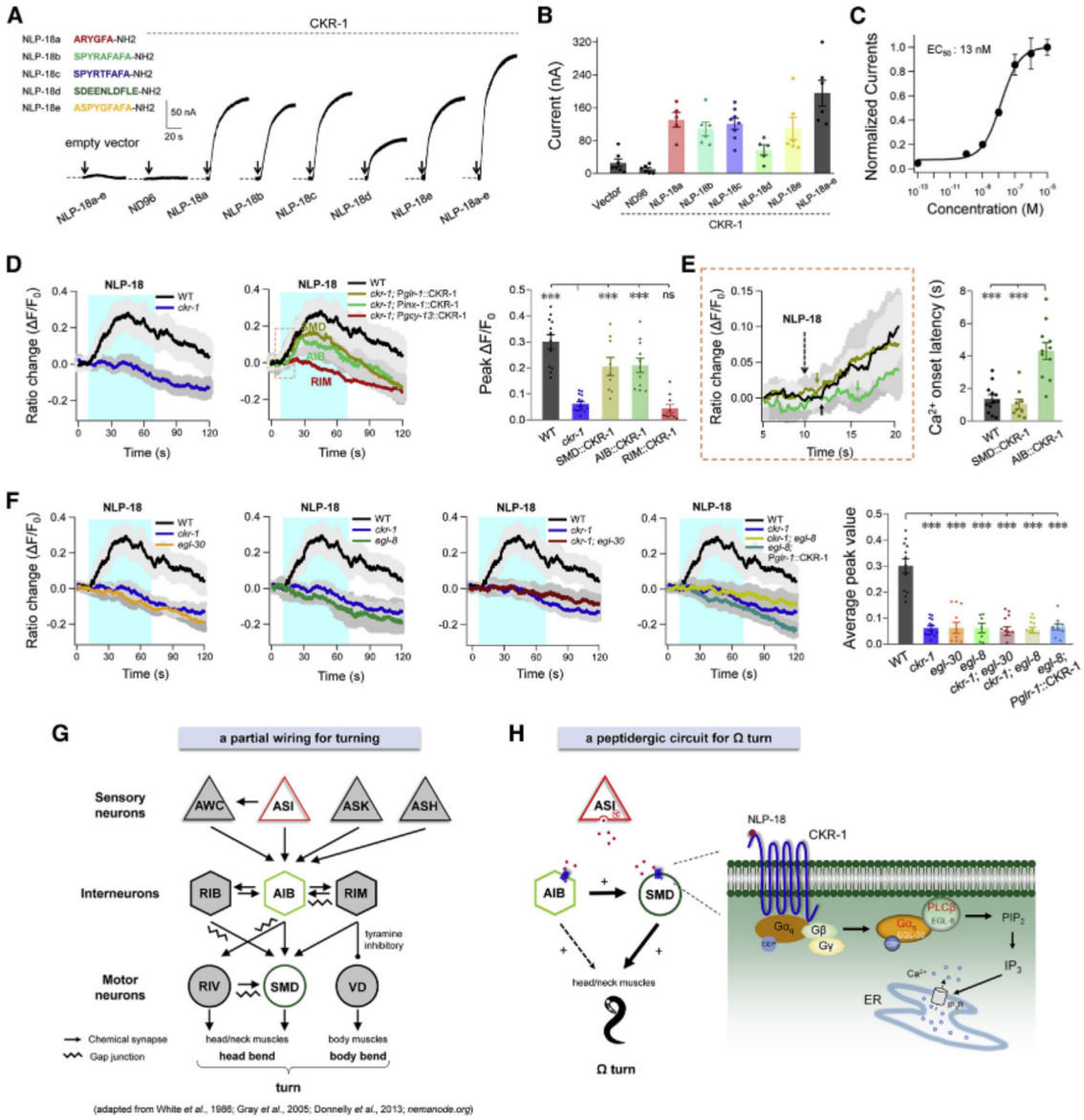

Figure 7. CKR-1 is a receptor of NLP-18

(A) Representative current traces evoked by different NLP-18 neuropeptides (1 μM) in the *Xenopus laevis* oocytes injected with CKR-1 cRNA. Five synthetic NLP-18 neuropeptides' sequences were denoted by colors (red NLP-18a, green NLP-18b, blue NLP-18c, dark green NLP-18d, and golden NLP-18e). Arrows indicate the puffing onset time.

(B) Quantification of the NLP-18-evoked peak currents ($n \geq 5$ oocytes).

(C) The dose response of the NLP-18a-evoked currents, revealing an EC_{50} of 13 nM fitted by Hill equation.

(D) NLP-18 neuropeptides (mixed NLP-18a–e; 1 μM each) evoked robust Ca^{2+} transient from the SMD neurons, which was terminated in the *ckr-1* mutant. The terminated Ca^{2+} transient could be rescued by expression of CKR-1 in SMD and AIB, but not in RIM, neurons ($n \geq 9$ animals). ***$p < 0.001$; Mann-Whitney test.

(E) A delayed activation occurred by expression of CKR-1 in AIB ($n \geq 9$ animals). ***$p < 0.001$; Mann-Whitney test.

(F) SMD Ca^{2+} transients evoked by NLP-18 mixed neuropeptides (NLP-18a–e; 1 μM each) exhibit remarkable decrease in *egl-30*, *egl-8* single mutant, and *ckr-1*; *egl-30* and *ckr-1*; *egl-8* double mutants. Expression of CKR-1 in SMD neurons could not rescue the Ca^{2+} response of *ckr-1* in *egl-8* mutant background ($n \geq 7$ animals). ***$p < 0.001$; Mann-Whitney test.

(G and H) Working model.

(G) Partial hard-wired neural circuit diagram for turning in *C. elegans*.

(H) A neuropeptidergic circuit and signaling pathway for Ω turn (escape steering): head-bending motor neuron SMD receives NLP-18-CKR-1 neuromodulation inputs from ASI and may simultaneously receive neurotransmission inputs from AIB (+). AIB strengthens the head muscle activity through SMD as well as other neurons (dash line). Sensory neurons are represented by triangles, interneurons by hexagons, and motor neurons by circles. Arrows represent connections via chemical synapses, which may be excitatory or inhibitory. Wave lines represent connections by electrical synapses.

Data are expressed as mean ± SEM.

and 10 nM and peak activation at 100 nM (Shigeri et al., 1996). NLP-12 was considered to be CCK-8's *C. elegans* homolog by sequence (Janssen et al., 2008), but *nlp-12* mutant animals do not exhibit escape-steering defect (Figure 1B). These findings argue for assessing physiological homology of peptidergic signaling by receptors instead of the primary sequence of ligands. Identifying NLP-18 as a cognate ligand further expands the search of multiple ligands for CCK receptors.

Peptidergic signaling functions through a hard-wired circuit

The steering behavior is regulated by sensory neurons, such as ASI (Figure 7G), that may not directly evoke escape responses. ASIs are gustatory and multimodal, known for their roles in food-related modulation, including insulin-related chemotaxis behaviors and dauer formation (Bargmann and Horvitz, 1991; Pandey et al., 2021; You et al., 2008). ASIs suppress Ω turn frequency by inhibiting the olfactory neuron AWC in the absence of food (Gray et al., 2005), in addition transducing noxious cues during nociception (Guo et al., 2015). This differs from the finding here that ASI is required for and enables steering by NLP-18-dependent increase of head motor neuron activity. We speculate that ASIs play dual roles: they are required for escape steering that is independent from food sensing but can activate a pathway to suppress Ω turn to allow food searching when animals are hungry.

NLP-18's target neurons are similarly specific. The head motor neurons SMDs' activity level determines Ω turn frequency (Gray et al., 2005), head-bend amplitude during foraging (Shen et al., 2016; Yeon et al., 2018), and post-reversal turn amplitude (Kaplan et al., 2020). Specific loss of elevated Ω-Ca^{2+} activity in SMD in *nlp-18* and *ckr-1* mutants demonstrates the requirement of peptidergic signaling. Intriguingly, depletion of CKR-1 in either SMD or AIB reduces escape steering. AIB interneurons transit animals from reversal to turn (Gray et al., 2005; Wang et al., 2020). By receiving chemical synapses from multiple sensory neurons, including ASI, they send chemical and electrical synapses to motor neurons SMDs. Because restoration of CKR-1 in AIB alone partially restored the escape-steering behavior and NLP-18-evoked SMD Ca^{2+} amplitude with a delay, AIB may promote escape steering through chemical synaptic activation of SMD (Figure 7H). Since ASIs have no direct connections to SMD neurons, the NLP-18-CKR-1 pathway may underlie a form of paracrine or endocrine signaling within the hard-wired neuronal circuit for escape. We propose that NLP-18-CKR-1 signaling strengthens the functional connection of the ASI-AIB-SMD circuit for robust escape steering.

RIM interneurons form a subcircuit with AIB, and they exhibit coordinated activity changes during reversal (Kawano et al., 2011). Ablation of RIM suppresses turnings during thermal taxis (Ji et al., 2021), but unlike the case of ASI ablation, *nlp-18*, and *ckr-1*, RIM's effect may be more context dependent. Although both *nlp-18* and *ckr-1* are expressed in RIM, depletion or overexpression of NLP-18 or CKR-1 in RIM did not change or rescue turning phenotypes of wild type or *nlp-18* or *ckr-1* mutants. Co-expression of NLP-18 in both ASI and RIM did achieve a slight improvement in behavior rescue compared with ASI alone, although we cannot rule out an overexpression effect. The lack of rescuing effect on its own may reflect its limited capacity for secreting NLP-18: unlike ASIs, RIMs exhibit mostly clear synaptic vesicles with a small number of dense core vesicles (Witvliet et al., 2021), supporting earlier work suggesting RIM is primarily a glutamatergic neuron (Alkema et al., 2005).

In summary, we identified a temporally and spatially controlled neuropeptidergic neuronal signaling pathway that functions in conjunction with hard-wired circuitry to drive escape steering. The head motor neuron that codes for turn angles requires this signaling to execute robust steering. With a specific input from a gustatory neuron to potentiate the interneurons and motor neurons that encode turning (Figure 7H), this wiring addition potentially renders food-state-dependent modulation of navigation.

Limitations of the study

We show here NLP-18-CKR's requirement for escape steering was independent of the type of stimuli or the environmental food signals. Because SMD motor neurons exhibit normal calcium dynamics during spontaneous backward movement in *nlp-18* and *ckr-1* mutants, these results support the notion that NLP-18 secretion occurs specifically during escape to regulate SMD and AIB for Ω turn. However, how this release is regulated remains unknown and requires further investigation.

STAR★METHODS

Detailed methods are provided in the online version of this paper and include the following:

- KEY RESOURCES TABLE
- RESOURCE AVAILABILITY
  - Lead contact
  - Materials availability
  - Data and code availability
- EXPERIMENTAL MODEL AND SUBJECT DETAILS
  - Animals
- METHOD DETAILS
  - Molecular biology
  - Transgenes arrays and strains
  - ZIF-1-ZF1 system
  - Neuronal manipulation
  - Behavioral analysis
  - Confocal fluorescence microscopy
  - Calcium imaging
  - Oocytes expression and electrophysiology
- QUANTIFICATION AND STATISTICAL ANALYSIS

SUPPLEMENTAL INFORMATION

Supplemental information can be found online at https://doi.org/10.1016/j.celrep.2022.110330.

ACKNOWLEDGMENTS

We thank Lijun Kang, Quan Wen, and Jianfeng Liu for comments and discussion. This research was supported by the Major International (Regional) Joint Research Project (32020103007), the National Natural Science Foundation of China (31871069), the Overseas High-Level Talents Introduction Program, and NSFC grant (31771294) to L.C. We thank the Caenorhabditis Genetics Center, which is funded by the NIH Office of Research Infrastructure Programs (P40 OD010440), for strains.

AUTHOR CONTRIBUTIONS

L.C. and S.G. conceived experiments, analyzed data, and wrote the manuscript. Y.L., P.S., Y.W., and Z.Y. performed experiments and analyzed data. W.H., H.L., M.-H.G., Z.-X.W., Y.Z., P.F., L.-M.C., L.T., and H.M. contributed to the experiments. M.Z. provided unpublished reagents, assisted with experimental design, and edited the text.

DECLARATION OF INTERESTS

The authors declare no competing interests.

Received: August 11, 2021
Revised: November 19, 2021
Accepted: January 11, 2022
Published: February 8, 2022

REFERENCES

Alkema, M.J., Hunter-Ensor, M., Ringstad, N., and Horvitz, H.R. (2005). Tyramine Functions independently of octopamine in the Caenorhabditis elegans nervous system. Neuron *46*, 247–260.

Armenti, S.T., Lohmer, L.L., Sherwood, D.R., and Nance, J. (2014). Repurposing an endogenous degradation system for rapid and targeted depletion of C. elegans proteins. Development *141*, 4640–4647.

Bargmann, C.I. (1998). Neurobiology of the Caenorhabditis elegans genome. Science *282*, 2028–2033.

Bargmann, C.I. (2012). Beyond the connectome: how neuromodulators shape neural circuits. Bioessays *34*, 458–465.

Bargmann, C.I., and Horvitz, H.R. (1991). Control of larval development by chemosensory neurons in Caenorhabditis elegans. Science *251*, 1243–1246.

Bargmann, C.I., and Marder, E. (2013). From the connectome to brain function. Nat. Methods *10*, 483–490.

Beinfeld, M.C. (1983). Cholecystokinin in the central nervous system: a minireview. Neuropeptides *3*, 411–427.

Berna, M.J., Tapia, J.A., Sancho, V., and Jensen, R.T. (2007). Progress in developing cholecystokinin (CCK)/gastrin receptor ligands that have therapeutic potential. Curr. Opin. Pharmacol. *7*, 583–592.

Bhardwaj, A., Thapliyal, S., Dahiya, Y., and Babu, K. (2018). FLP-18 functions through the G-protein-coupled receptors NPR-1 and NPR-4 to modulate reversal length in Caenorhabditis elegans. J. Neurosci. *38*, 4641–4654.

Blitz, D.M., and Nusbaum, M.P. (2008). State-dependent presynaptic inhibition regulates central pattern generator feedback to descending inputs. J. Neurosci. *28*, 9564–9574.

Broekmans, O.D., Rodgers, J.B., Ryu, W.S., and Stephens, G.J. (2016). Resolving coiled shapes reveals new reorientation behaviors in C. elegans. Elife *5*, e17227.

Chalfie, M., and Jorgensen, E.M. (1998). C. elegans neuroscience: genetics to genome. Trends Genet. *14*, 506–512.

Chalfie, M., Sulston, J.E., White, J.G., Southgate, E., Thomson, J.N., and Brenner, S. (1985). The neural circuit for touch sensitivity in Caenorhabditis elegans. J. Neurosci. *5*, 956–964.

Cook, S.J., Jarrell, T.A., Brittin, C.A., Wang, Y., Bloniarz, A.E., Yakovlev, M.A., Nguyen, K.C.Q., Tang, L.T., Bayer, E.A., Duerr, J.S., et al. (2019). Whole-animal connectomes of both Caenorhabditis elegans sexes. Nature *571*, 63–71.

Croll, N.A. (1975). Behavioural analysis of nematode movement. Adv. Parasitol. *13*, 71–122.

Donnelly, J.L., Clark, C.M., Leifer, A.M., Pirri, J.K., Haburcak, M., Francis, M.M., Samuel, A.D., and Alkema, M.J. (2013). Monoaminergic orchestration of motor programs in a complex C. elegans behavior. PLoS Biol. *11*, e1001529.

Dufresne, M., Seva, C., and Fourmy, D. (2006). Cholecystokinin and gastrin receptors. Physiol. Rev. *86*, 805–847.

Dunn, T.W., Gebhardt, C., Naumann, E.A., Riegler, C., Ahrens, M.B., Engert, F., and Del Bene, F. (2016). Neural circuits underlying visually evoked escapes in larval zebrafish. Neuron *89*, 613–628.

Fotowat, H., and Gabbiani, F. (2011). Collision detection as a model for sensory-motor integration. Annu. Rev. Neurosci. *34*, 1–19.

Friedrich, R.W. (2013). Neuronal computations in the olfactory system of zebrafish. Annu. Rev. Neurosci. *36*, 383–402.

Friesen, W.O., and Kristan, W.B. (2007). Leech locomotion: swimming, crawling, and decisions. Curr. Opin. Neurobiol. *17*, 704–711.

Frooninckx, L., Van Rompay, L., Temmerman, L., Van Sinay, E., Beets, I., Janssen, T., Husson, S.J., and Schoofs, L. (2012). Neuropeptide GPCRs in C. elegans. Front Endocrinol. (Lausanne) *3*, 167.

Gordus, A., Pokala, N., Levy, S., Flavell, S.W., and Bargmann, C.I. (2015). Feedback from network states generates variability in a probabilistic olfactory circuit. Cell *161*, 215–227.

Gray, J.M., Hill, J.J., and Bargmann, C.I. (2005). A circuit for navigation in Caenorhabditis elegans. Proc. Natl. Acad. Sci. U S A *102*, 3184–3191.

Grillner, S., and Jessell, T.M. (2009). Measured motion: searching for simplicity in spinal locomotor networks. Curr. Opin. Neurobiol. *19*, 572–586.

Guo, M., Wu, T.H., Song, Y.X., Ge, M.H., Su, C.M., Niu, W.P., Li, L.L., Xu, Z.J., Ge, C.L., Al-Mhanawi, M.T., et al. (2015). Reciprocal inhibition between sensory ASH and ASI neurons modulates nociception and avoidance in Caenorhabditis elegans. Nat. Commun. *6*, 5655.

Harris-Warrick, R.M. (2011). Neuromodulation and flexibility in central pattern generator networks. Curr. Opin. Neurobiol. *21*, 685–692.

Hendricks, M., Ha, H., Maffey, N., and Zhang, Y. (2012). Compartmentalized calcium dynamics in a C. elegans interneuron encode head movement. Nature *487*, 99–103.

Hilliard, M.A., Apicella, A.J., Kerr, R., Suzuki, H., Bazzicalupo, P., and Schafer, W.R. (2005). In vivo imaging of C. elegans ASH neurons: cellular response and adaptation to chemical repellents. EMBO J. *24*, 63–72.

Hu, Z., Pym, E.C., Babu, K., Vashlishan Murray, A.B., and Kaplan, J.M. (2011). A neuropeptide-mediated stretch response links muscle contraction to changes in neurotransmitter release. Neuron *71*, 92–102.

Husson, S.J., and Schoofs, L. (2007). Altered neuropeptide profile of Caenorhabditis elegans lacking the chaperone protein 7B2 as analyzed by mass spectrometry. FEBS Lett. *581*, 4288–4292.

Ivy, A.C., and Oldberg, E. (1928). A hormone mechanism for gall-bladder contraction and evacuation. Am. J. Physiol. *86*, 455–599.

Jacob, T.C., and Kaplan, J.M. (2003). The EGL-21 carboxypeptidase E facilitates acetylcholine release at Caenorhabditis elegans neuromuscular junctions. J. Neurosci. *23*, 2122–2130.

Jansen, G., Thijssen, K.L., Werner, P., van der Horst, M., Hazendonk, E., and Plasterk, R.H. (1999). The complete family of genes encoding G proteins of Caenorhabditis elegans. Nat. Genet. *21*, 414–419.

Janssen, T., Lindemans, M., Meelkop, E., Temmerman, L., and Schoofs, L. (2010). Coevolution of neuropeptidergic signaling systems: from worm to man. Ann. N. Y Acad. Sci. *1200*, 1–14.

Janssen, T., Meelkop, E., Lindemans, M., Verstraelen, K., Husson, S.J., Temmerman, L., Nachman, R.J., and Schoofs, L. (2008). Discovery of a cholecystokinin-gastrin-like signaling system in nematodes. Endocrinology *149*, 2826–2839.

Jensen, R.T. (2002). Involvement of cholecystokinin/gastrin-related peptides and their receptors in clinical gastrointestinal disorders. Pharmacol. Toxicol. *91*, 333–350.

Ji, N., Venkatachalam, V., Rodgers, H.D., Hung, W., Kawano, T., Clark, C.M., Lim, M., Alkema, M.J., Zhen, M., and Samuel, A.D. (2021). Corollary discharge promotes a sustained motor state in a neural circuit for navigation. Elife *10*, e68848.

Kagawa-Nagamura, Y., Gengyo-Ando, K., Ohkura, M., and Nakai, J. (2018). Role of tyramine in calcium dynamics of GABAergic neurons and escape behavior in Caenorhabditis elegans. Zoological. Lett. *4*, 19.

Kaplan, H.S., Salazar Thula, O., Khoss, N., and Zimmer, M. (2020). Nested neuronal dynamics orchestrate a behavioral hierarchy across timescales. Neuron *105*, 562–576 e569.

Kass, J., Jacob, T.C., Kim, P., and Kaplan, J.M. (2001). The EGL-3 proprotein convertase regulates mechanosensory responses of Caenorhabditis elegans. J. Neurosci. *21*, 9265–9272.

Katz, P.S. (2016). Evolution of central pattern generators and rhythmic behaviours. Philos. Trans. R. Soc. Lond. B Biol. Sci. *371*, 20150057.

Kawano, T., Po, M.D., Gao, S., Leung, G., Ryu, W.S., and Zhen, M. (2011). An imbalancing act: gap junctions reduce the backward motor circuit activity to bias C. elegans for forward locomotion. Neuron *72*, 572–586.

Li, C., and Kim, K. (2008). Neuropeptides. WormBook, 1–36. http://www.wormbook.org/chapters/www_neuropeptides/neuropeptides.html.

Li, C., and Kim, K. (2010). Neuropeptide gene families in Caenorhabditis elegans. Adv. Exp. Med. Biol. *692*, 98–137.

Li, W., Kang, L., Piggott, B.J., Feng, Z., and Xu, X.Z. (2011). The neural circuits and sensory channels mediating harsh touch sensation in Caenorhabditis elegans. Nat. Commun. *2*, 315.

Lim, M.A., Chitturi, J., Laskova, V., Meng, J., Findeis, D., Wiekenberg, A., Mulcahy, B., Luo, L., Li, Y., Lu, Y., et al. (2016). Neuroendocrine modulation sustains the C. elegans forward motor state. Elife *5*, e26528.

Magnani, E., Bartling, L., and Hake, S. (2006). From gateway to multisite gateway in one recombination event. BMC Mol. Biol. *7*, 46.

Maguire, S.M., Clark, C.M., Nunnari, J., Pirri, J.K., and Alkema, M.J. (2011). The C. elegans touch response facilitates escape from predacious fungi. Curr. Biol. *21*, 1326–1330.

Marder, E., and Bucher, D. (2001). Central pattern generators and the control of rhythmic movements. Curr. Biol. *11*, R986–R996.

Marder, E., O'Leary, T., and Shruti, S. (2014). Neuromodulation of circuits with variable parameters: single neurons and small circuits reveal principles of state-dependent and robust neuromodulation. Annu. Rev. Neurosci. *37*, 329–346.

Meelkop, E., Temmerman, L., Janssen, T., Suetens, N., Beets, I., Van Rompay, L., Shanmugam, N., Husson, S.J., and Schoofs, L. (2012). PDF receptor signaling in Caenorhabditis elegans modulates locomotion and egg-laying. Mol. Cell Endocrinol. *361*, 232–240.

Miller, A.C., Whitebirch, A.C., Shah, A.N., Marsden, K.C., Granato, M., O'Brien, J., and Moens, C.B. (2017). A genetic basis for molecular asymmetry at vertebrate electrical synapses. Elife *6*, e25364.

Nassel, D.R. (2009). Neuropeptide signaling near and far: how localized and timed is the action of neuropeptides in brain circuits? Invert Neurosci. *9*, 57–75.

Oranth, A., Schultheis, C., Tolstenkov, O., Erbguth, K., Nagpal, J., Hain, D., Brauner, M., Wabnig, S., Steuer Costa, W., McWhirter, R.D., et al. (2018). Food sensation modulates locomotion by dopamine and neuropeptide signaling in a distributed neuronal network. Neuron *100*, 1414–1428 e1410.

Oron, Y., Dascal, N., Nadler, E., and Lupu, M. (1985). Inositol 1,4,5-trisphosphate mimics muscarinic response in Xenopus oocytes. Nature *313*, 141–143.

Pandey, P., Bhat, U.S., Singh, A., Joy, A., Birari, V., Kadam, N.Y., and Babu, K. (2021). Dauer formation in C. elegans is modulated through AWC and ASI-dependent chemosensation. eNeuro *8*, ENEURO.0473-20.2021.

Pierce, S.B., Costa, M., Wisotzkey, R., Devadhar, S., Homburger, S.A., Buchman, A.R., Ferguson, K.C., Heller, J., Platt, D.M., Pasquinelli, A.A., et al. (2001). Regulation of DAF-2 receptor signaling by human insulin and ins-1, a member of the unusually large and diverse C. elegans insulin gene family. Genes Dev. *15*, 672–686.

Piggott, B.J., Liu, J., Feng, Z., Wescott, S.A., and Xu, X.Z. (2011). The neural circuits and synaptic mechanisms underlying motor initiation in C. elegans. Cell *147*, 922–933.

Pirri, J.K., and Alkema, M.J. (2012). The neuroethology of C. elegans escape. Curr. Opin. Neurobiol. *22*, 187–193.

Pirri, J.K., McPherson, A.D., Donnelly, J.L., Francis, M.M., and Alkema, M.J. (2009). A tyramine-gated chloride channel coordinates distinct motor programs of a Caenorhabditis elegans escape response. Neuron *62*, 526–538.

Pokala, N., Liu, Q., Gordus, A., and Bargmann, C.I. (2014). Inducible and titratable silencing of Caenorhabditis elegans neurons in vivo with histamine-gated chloride channels. Proc. Natl. Acad. Sci. U S A *111*, 2770–2775.

Qi, Y.B., Garren, E.J., Shu, X., Tsien, R.Y., and Jin, Y. (2012). Photo-inducible cell ablation in Caenorhabditis elegans using the genetically encoded singlet oxygen generating protein miniSOG. Proc. Natl. Acad. Sci. U S A *109*, 7499–7504.

Rogers, C., Reale, V., Kim, K., Chatwin, H., Li, C., Evans, P., and de Bono, M. (2003). Inhibition of *Caenorhabditis elegans* social feeding by FMRFamide-related peptide activation of NPR-1. Nat. Neurosci. *6*, 1178–1185.

Sakurai, T. (2007). The neural circuit of orexin (hypocretin): maintaining sleep and wakefulness. Nat. Rev. Neurosci. *8*, 171–181.

Shen, Y., Wen, Q., Liu, H., Zhong, C., Qin, Y., Harris, G., Kawano, T., Wu, M., Xu, T., Samuel, A.D., et al. (2016). An extrasynaptic GABAergic signal modulates a pattern of forward movement in Caenorhabditis elegans. Elife *5*, e14197.

Shigeri, Y., Shinohara, S., Murata, S., Fujimoto, M., and Kawasaki, K. (1996). Expression of two different cholecystokinin receptors in Xenopus oocytes injected with mRNA from rabbit pancreas and rat hippocampus. Jpn. J. Pharmacol. *72*, 9–15.

Shintaku, H., Katsuura, G., Katoh, A., Eigyo, M., and Matsushita, A. (1992). A possible involvement of CCK-A receptor in ceru 1 etide-induced protection against neuronal cell death following cerebral ischemia in Mongolian gerbils. Jpn. J. Pharmacol., 253.

Shu, X., Lev-Ram, V., Deerinck, T.J., Qi, Y., Ramko, E.B., Davidson, M.W., Jin, Y., Ellisman, M.H., and Tsien, R.Y. (2011). A genetically encoded tag for correlated light and electron microscopy of intact cells, tissues, and organisms. PLoS Biol. *9*, e1001041.

Taylor, S.R., Santpere, G., Weinreb, A., Barrett, A., Reilly, M.B., Xu, C., Varol, E., Oikonomou, P., Glenwinkel, L., McWhirter, R., et al. (2021). Molecular topography of an entire nervous system. Cell *184*, 4329–4347 e4323.

Wakabayashi, T., Kitagawa, I., and Shingai, R. (2004). Neurons regulating the duration of forward locomotion in Caenorhabditis elegans. Neurosci. Res. *50*, 103–111.

Wang, Y., Zhang, X., Xin, Q., Hung, W., Florman, J., Huo, J., Xu, T., Xie, Y., Alkema, M.J., Zhen, M., et al. (2020). Flexible motor sequence generation during stereotyped escape responses. Elife *9*, e56942.

White, J.G., Southgate, E., Thomson, J.N., and Brenner, S. (1986). The structure of the nervous system of the nematode Caenorhabditis elegans. Philos. Trans. R. Soc. Lond. B Biol. Sci. *314*, 1–340.

Wicks, S.R., Roehrig, C.J., and Rankin, C.H. (1996). A dynamic network simulation of the nematode tap withdrawal circuit: predictions concerning synaptic function using behavioral criteria. J. Neurosci. *16*, 4017–4031.

Witvliet, D., Mulcahy, B., Mitchell, J.K., Meirovitch, Y., Berger, D.R., Wu, Y., Liu, Y., Koh, W.X., Parvathala, R., Holmyard, D., et al. (2021). Connectomes across development reveal principles of brain maturation. Nature *596*, 257–261.

Ye, H., Hui, L., Kellersberger, K., and Li, L. (2013). Mapping of neuropeptides in the crustacean stomatogastric nervous system by imaging mass spectrometry. J. Am. Soc. Mass. Spectrom. *24*, 134–147.

Yeon, J., Kim, J., Kim, D.Y., Kim, H., Kim, J., Du, E.J., Kang, K., Lim, H.H., Moon, D., and Kim, K. (2018). A sensory-motor neuron type mediates proprioceptive coordination of steering in C. elegans via two TRPC channels. PLoS Biol. *16*, e2004929.

You, Y.J., Kim, J., Raizen, D.M., and Avery, L. (2008). Insulin, cGMP, and TGF-beta signals regulate food intake and quiescence in C. elegans: a model for satiety. Cell Metab. *7*, 249–257.

Zhao, B., Khare, P., Feldman, L., and Dent, J.A. (2003). Reversal frequency in Caenorhabditis elegans represents an integrated response to the state of the animal and its environment. J. Neurosci. *23*, 5319–5328.

STAR★METHODS

KEY RESOURCES TABLE

REAGENT or RESOURCE	SOURCE	IDENTIFIER
Bacterial and virus strains		
OP50	CGC	http://www.cgc.edu/strain/OP50
Chemicals, peptides, and recombinant proteins		
NLP-18a	Guoping Pharmaceutical Company	ARYGFA-NH2
NLP-18b	Guoping Pharmaceutical Company	SPYRAFAFA-NH2
NLP-18c	Guoping Pharmaceutical Company	SPYRTFAFA-NH2
NLP-18d	Guoping Pharmaceutical Company	SDEENLDFLE-NH2
NLP-18e	Guoping Pharmaceutical Company	ASPYGFAFA-NH2
ClonExpress®II One Step Cloning Kit	Vazyme Biotech co., ltd	Vazyme#C112
2 × Phanta® Max Master Mix (Dye Plus)	Vazyme Biotech co., ltd	Vazyme#P525
Gateway™ LR Clonase™ Plus Enzyme Mix	Invitrogen, Thermo Fisher Scientific	Cat#12538-013
BP Clonase™ II Enzyme Mix	Invitrogen, Thermo Fisher Scientific	Cat#11789-013
Experimental models: Organisms/strains		
C. elegans strain, see Table S1	This paper	N/A
Oligonucleotides		
See Table S3	This paper	N/A
Recombinant DNA		
See Table S2	This paper	N/A
Software and algorithms		
ImageJ	National Institutes of Health	https://imagej.nih.gov/ij/
Matlab	MathWorks	https://ww2.mathworks.cn/products/matlab.html
Clampfit	Molecular Devices	https://www.moleculardevices.com/p
Vector NTI	Thermo Fisher Scientific	https://www.thermofisher.cn/
GraphPad Prism 8	GraphPad Software Inc.	https://www.graphpad.com/
Igor Pro	WaveMetrics	https://www.wavemetrics.com/
MEGA 6.60	Molecular Evolutionary Genetics Analysis	https://megasoftware.net/

RESOURCE AVAILABILITY

Lead contact

Further information and requests for resources and reagents should be directed to and will be fulfilled by the lead contact, Shangbang Gao (sgao@hust.edu.cn).

Materials availability

All unique reagents generated in this study are available from the lead contact with a completed materials transfer agreement.

Data and code availability

All data reported in this paper will be shared by the lead contact upon request.

This paper does not report original code.

Any additional information required to reanalyze the data reported in this paper is available from the lead contact upon request.

EXPERIMENTAL MODEL AND SUBJECT DETAILS

Animals

C. elegans strains were cultured on the standard Nematode Growth Medium (NGM) plates seeded with OP50 and maintained at 22°C. Unless otherwise stated, the wild-type animal refers to the Bristol N2 strain. L4 stage or young adults (24 h post L4 stage) hermaphrodites were used in all experiments. Other genetic mutants used for constructing transgenic lines and compound mutants

were obtained from the *Caenorhabditis Genetics Center (CGC)*. The complete lists of transgenic lines and strains generated or acquired for this study are provided in Table S1.

METHOD DETAILS

Molecular biology

All expression plasmids in this study were constructed by Three-Fragment Multisite gateway (Invitrogen, Thermo Fisher Scientific, Waltham, MA, USA) (Magnani et al., 2006). Three-Fragment Multisite gateway system consists of three entry clones. Three entry clones comprising three PCR products (promoter, gene of interest, *sl2d*-GFP, *sl2d*-wCherry or *unc-54*-3′UTR, in name of slot1, slot2 and slot3, respectively) were recombined into the *pDEST-R4-R3*, *pDEST-R4-R3-unc-54* 3′UTR, *pBCN44-R4R3-Plin-44*:GFP and *pBCN44-R4R3-Pvha-6*:GFP destination vectors by using standard LR recombination reactions to generate the expression clones.

All promoters used in this study were generated by PCR against a mixed-stage N2 *C. elegans* genomic DNA. Promoters' genomic sequences were used to substitute for the *rab-3* fragment in standard BP reaction-generated entry clone A with the In-Fusion method, using ClonExpress®IIOne Step Cloning Kit.

To generate the entry clones slot2 and slot3, we used standard BP recombination reactions. An entry clone B contributing sequences of slot 2 in the expression plasmid contains sequence of a target gene, i.e., *nlp-18*, *ckr-1*, or any gene of interest. The "B" entry clones were constructed by using of *pDONR^{TM} 221* donor vector (Invitrogen) through BP reactions. All the DNA fragments used to construct entry clone B involved in this project were amplified by PCR with the primers containing attB1 and attB2 recombination sites.

An entry clone C contributing sequences of slot 3 in the expression plasmids contains a sequence of *unc-54*-3′UTR, *sl2d*-GFP or *sl2d*-wCherry. The "C" entry clones were constructed by use of *pDONR-P2R-P3* donor vector through standard BP reactions. The corresponding PCR products with attB2R and attB3 sites were amplified by PCR. The "C" entry clones containing *unc-54*-3′UTR, *sl2d*-GFP and *sl2d*-wCherry were used to construct expression plasmids.

Transgenes arrays and strains

Transgenic animals that carry non-integrated, extra-chromosomal arrays (*gaaEx*) were generated by co-injecting an injection marker with one to multiple DNA construct at 5–30 ng/μL. Animals that carry integrated transgenic arrays (*gaaIs*) were generated from the *gaaEx* animals by UV irradiation, followed by outcrossing against N2 at least 4 times.

ZIF-1-ZF1 system

ZIF-1-ZF1 system was used to degrade target protein in specific tissue and neurons respectively (Armenti et al., 2014). In ZIF-1-ZF1 system, P*ckr-1*-ZF1-SL2-NLS-GFP was knocked in before termination codon of *ckr-1* using CRISPR-Cas9 to generate GB01 *gaaIs1* (P*ckr-1*-ZF1-SL2-NLS-GFP) strain. Using different promoter combined ZIF-1 and *sl2d*-GFP or *sl2d*-wCherry by LR reaction to construct expression plasmids then co-injecting P*lin-44*:GFP into GB01 to degrade CKR-1 protein in specific neuron.

Neuronal manipulation

To dissect the role of ASI neurons in locomotion modulation, we expressed mito-miniSOG into these neurons driven by P*gpa-4*. Ablation of ASIs was performed using a homemade LED box, where the standard NGM were exposed under a homemade 470 nm blue LED light (8.3 mW/cm^2) for 30–45 min. To monitor the specificity and efficacy of cell ablation, cytoplasmic wCherry was co-expressed with miniSOG (tomm-20-miniSOG-SL2-wCherry) in targeted neurons by the same promoter. Ablation was performed when animals were in the L2-L3 stage, which would be examined whether the wCherry fluorescence was absent after 24 h. Late L4 or young adult stage animals were recorded for behavioral analysis.

For chemogenetic silencing the ASI neurons, we used neuronal specific promoter P*gpa-4* to drive expression of the Drosophila *HisCl* gene in the ASI neurons. To make NGM-HA plates, histamine (Sigma Aldrich histamine-dihydrochloride, 1 M stock in water) was added to NGM agar at ~65°C. Histamine-free control plates were poured from the same NGM batch. NGM plates with 10 mM histamine were used to test the behavioral effects.

Behavioral analysis

Harsh head touch was delivered with a platinum wire pick. One hour prior to testing, normal cultured young adult hermaphroditic animals (8–12 h post L4 stage) were transferred to plates with thin layer of OP50 bacteria. The worm head was touched with the edge in a top-down manner with a force of 100–200 μN (Li et al., 2011). For each strain, at least 30 worms were recorded in each group and experiment was repeated for 3–5 times. To avoid the possible stimulation-induced adaptation, each worm was tested for one time. The full omega was defined as the head contact with the body when animal turning after reversal, or else it was classified into shallow omega. A part of animals (2.7 ± 0.4%) did not execute the omega turn but only reversal after stimulation. The proportion of full omega, shallow omega and only reversal was quantified to present the robustness of escape behavior. Omega curvature analysis utilized image J (National Institutes of Health) and Matlab (MathWorks). Extracting image which worm started to enter turning and showed the largest bending of head. Images from each animal were divided into 50 body segments for curvature analysis.

The curvatures at each point along the worm centerline $k(s)$ can be calculated with the coordinate of each point ($x(s)$, $y(s)$) using the formula $k(s) = \frac{x'y'' - x''y'}{(x'^2 + y'^2)^{(3/2)}}$ where s is the normalized location along centerline (head = 0, tail = 1), and the unit of k is pixel^(-1). Then k is normalized with the length of worm body L, resulting in the dimensionless $k\sim(s)$ using the formula $\tilde{k}(s) = k(s) \times L$. The curvature from 0% to 60% body segment was plotted and converted as a color map. Omega angle was defined as the intersection angle from middle point of body (the 26th cross line) to the closest points anterior and posterior of the animal. Thus, the angle of full omega is zero degree.

A single young adult hermaphrodite (12–18 h post L4 stage), maintained on standard culture conditions, was transferred to a 60 mm imaging plate seeded with a thin layer of OP50. One minute after the transfer, a three-minute video of the crawling animal was recorded on a modified stereo microscope (Axio Zoom V16, Zeiss) with a digital camera (acA2500-60um, Basler). Post-imaging analysis utilized an in-house written MATLAB script. The central line was used to track. Images for velocity analysis from each animal were divided into 33 body segments. The mid-point was used to calculate the velocity and direction of movements between each frame.

Imaging plates were prepared as follows: a standard NGM plate was seeded with a thin layer of OP50 12–14 h before the experiment. Immediately before the transfer of worms, the OP50 lawn was spread evenly across the plate with a sterile bent glass rod. All images were captured with a 10× objective at 10 Hz.

Confocal fluorescence microscopy

L4 stage transgenic animals expressing fluorescence markers were picked a day before imaging. Worms were immobilized by 2.5 mM levamisole (Sigma-Aldrich) in M9 buffer. Fluorescence signals were captured from live worms using a Plan-Apochromatic 60× objective on a confocal microscope (FV3000, Olympus) in the same conditions. Figures 2C and 4A panels are composite images of several mounted microphotographs to present a complete view of the worm.

Calcium imaging

The free-tracking Ca^{2+} imaging system include two independent modules: behavior tracking system and fluorescence recording system. Worm behavior was imaged under dark-field illumination in the near-infrared (NIR). Pick a worm on 6 cm NGM plates and then put it on a THOPLABS spw602 XY motorized stage controlled. Imaging plates were prepared according to the behavior imaging plates. Tracking imaging was conducted using a 10× inverted objective (Olympus, Japan) and recorded using a CCD camera (Point Gray Research, CM3-U3-13S2M, Canada). Custom real-time computer vision software kept the worm centered in the field of view via tracing centerline of worm. Fluorescence recording system records neuronal Ca^{2+} activity by using sCMOS digital camera (Hamamatsu, Japan) with 20× objective (Olympus, Japan). To simultaneously image wCherry and GCaMP6 side-by-side, we used a two-channel imager (W-VIEW GEMINI, Japan). Red and green channel fluorescent images were recorded simultaneously at 8 fps with 10 ms and 70 ms exposure time, respectively. Fluorescent images were captured using HCImage software (Hamamatsu). Neural activity was reported as normalized deviations from baseline of the ratio between GCaMP6s and wCherry fluorescence, $\Delta R/R_0 = R - R_0/R_0,$ where $R = I_{GCaMP6}/I_{wCherry}$. The baseline R_0 is defined as the minimum of R. The intensities $I_{GCaMP6s}$ and $I_{wCherry}$ were measured as the pixel intensity in the green and red channels, respectively. Custom MATLAB scripts were used to extract the pixel intensity for each frame. We focused on SMDD for quantitative analysis was that in our reporter, SMDD was isolated from other neurons when compared to SMDV, making it easier to extract high-quality activity traces. On a side note, we noticed that when we performed calcium imaging recordings, it was not difficult to find animals executing dorsal Ω turns, which occurs much less frequently under regular light microscopy.

For NLP-18 puffing evoked Ca^{2+} imaging, worms were glued and dissected to expose SMD neuron as described for electrophysiological recording. Then imaged with a 60× water objective (Nikon, Japan) and sCMOS digital camera (Hamamatsu ORCA-Flash 4.0 V2, Japan) at 10 Hz with expose time 100 ms. For all the SMD puffing neuropeptides experiments, we recorded the neuronal Ca^{2+} transient by the perfusion of the NLP-18 neuropeptides for 60 s and washing out for 50 s by normal bath solution. Ca^{2+} transients' onset latency was calculated by the time difference from the perfusion onset to Ca^{2+} initiation. The Ca^{2+} transients of SMD soma were analyzed by Image-Pro Plus 6 (Media Cybernetics, Inc., Rockville, MD, USA).

Oocytes expression and electrophysiology

CKR-1 expression in *X. laevis oocytes*: CKR-1 cDNAs were flanked between BamHI and HindIII sites by PCR and cloned into the *pGH19* vector. CKR-1 cRNAs were prepared using the mMessage Machine kit (Ambion). *X. laevis* oocytes were injected with 50 ng of CKR-1 receptor sense cRNAs. Injected oocytes were then incubated at 18°C in the ND96 medium for 2–3 days before recording.

Current recordings were made using the two-electrode voltage-clamp technique at a holding potential of −80 mV as described (Rogers et al., 2003). Oocytes were continuously superfused with ND96 solution contains: 96 mM NaCl, 2.5 mM KCl, 1 mM $MgCl_2$ and 5 mM HEPES, pH 7.3. The recording chamber was perfused with high-K^+ solution to reverse the K^+ gradient (Rogers et al., 2003) and measured the ligands (NLP-18a-e) dependent outward Ca^{2+}-gated chloride currents (Oron et al., 1985). The pipette solution contains 3 M KCl. The recording high-K^+ bath solution contains: 96 mM KCl, 2.5 mM NaCl, 1 mM $MgCl_2$ and 5 mM HEPES, pH 7.3. Peptide perfusion was terminated by washout with high-K^+ solution and subsequent switching to ND96 solution. Data were

acquired with Clampex 8.0 software (Molecular Devices) and analyzed offline with Clampfit (Molecular Devices). Peptides were synthesized by the Guoping Pharmaceutical Company (Hefei, Anhui Province, China).

QUANTIFICATION AND STATISTICAL ANALYSIS

The Mann-Whitney test, two-tailed Student's t-test, Two-way analysis of variance (ANOVA) tested were used to compare datasets. Statistical analysis of proportion was performed with the Fisher's exact test. Kolmogorov-Smirnov was used analysis shallow exit Ω angle cumulative fraction. The paired Ca^{2+} values from same SMDD neurons were analyzed by Wilcoxon matched-pairs signed rank test. Two-way analysis of variance was used to examine the effect of different genotype and body segment (two factors) on the entry Ω curvature by using the F-test for statistical significance. The F-test is a groupwise comparison test, which means it compares the variance in each group mean to the overall variance in the dependent variable. All data are presented as mean ± SEM. Above all statistical analysis were performed using GraphPad Prism 8 (GraphPad Software Inc.). $p < 0.05$ was considered to be statistically significant (*$p < 0.05$, **$p < 0.01$, ***$p < 0.001$). Graphing was performed using Igor Pro (WaveMetrics), Clampfit (Molecular Devices), ImageJ (National Institutes of Health), Matlab (MathWorks), GraphPad Prism 8 (GraphPad Software Inc.). Phylogenetic tree was analyzed by MEGA 6.60. For behavior analysis and fluorescence imaging, unless specified otherwise, each recording trace was obtained from a different animal.